Zircon U-Pb Geochronology from Ledge Mountain, Adirondack Highlands, New York

A Thesis submitted to the faculty of
San Francisco State University
In partial fulfillment of
the requirements for
the Degree

Master of Science

In

Geoscience

by

Laura Pauline Horsley

San Francisco, California

December 2023

Certificate of Approval

I certify that I have read Zircon U-Pb Geochronology from Ledge Mountain, Adirondacks Highlands, New York by Laura Pauline Horsley, and that in my opinion this work meets the criteria for approving a thesis submitted in partial fulfillment of the requirement for the degree Master of Science in Geoscience at San Francisco State University.

Mary Leech, PhD
Professor
Thesis Committee Chair

Alexander Stine, PhD
Professor

Ellen Metzger, PhD
Professor

Abstract

I use a combination of U-Pb SHRIMP zircon geochronology and trace element geochemistry, and interpreted cathodoluminescence imagery of zircons, to better constrain the timing of metamorphism and anatexis in migmatitic granulites from the central Adirondack Highlands. The Adirondack Highlands are a southern extension of the ca. 1 Ga Grenville Province, an orogen that stretches from northeastern Canada to western Texas. The Adirondack Highlands experienced ultrahigh-temperature (UHT) granulite-facies metamorphism and migmatization during the Shawinigan and Ottawan orogenic events within the Grenville. Ledge Mountain migmatites and Snowy Mountain and Oregon anorthosite massifs are part of a proposed gneiss dome that exhumed deep crustal rocks. Migmatite samples are from the western branch of Ledge Mountain and contain rounded, subhedral, to elongate zircons in both the leucosome and the melanosome. In cathodoluminescence (CL) imagery, zircons have thin dark homogeneous rims and core domains with variable CL and a range of textures. Most notable are the zircon domains featuring chaotic zoning with brightnesses ranging from bright to dark and chaotic textures. Faded oscillatory zoning patterns (OZP) were identified in many zircon cores and represent recrystallization that has resulted in a diffusion of igneous OZP. Homogenous zircon textures indicate recrystallization after an anatectic melt from 1037 ± 0.2 to 1029 ± 0.3 Ma. Chaotic zircon textures suggest fluid driven recrystallization during the anatexis and exhumation of the gneiss dome with U-Pb mean ages ranging from 1056 ± 0.2 to 1045 ± 0.3 Ma. These zircon ages suggest metamorphism continued into the mid- to late-Ottawan in the central Highlands and further constrained the timing of the exhumation of these deep crustal rocks.

Acknowledgements

This research was funded by the Department of Earth & Climate Sciences Pestrong Fund, the USGS EDMAP program, and the ARCS Foundation scholarship. Thank you to my field partners, Zach Smirnov and Victoria Hicks, for their assistance in the field. Thanks to Matt Coble and the staff in the SHRIMP-RG lab at Stanford University. And the biggest thanks go to my advisor, Dr. Mary Leech. This was the toughest thing I have ever attempted to accomplish and I barely made it through. I can honestly say I could not have done it without you. Thank you for your plentiful patience and endless wisdom.

Table of Contents

List of Tables

List of Figures

List of Appendices

INTRODUCTION

Zircons from Ledge Mountain (LM) migmatites have preserved textures that are indicative of metamorphic and magmatic events from orogenic events during the Grenvillian orogeny 1 Ga. Microtextural analysis from cathodoluminescence (CL) imaging along with mineral geochemistry and U-Pb SHRIMP zircon geochronology age dating can constrain the timing of these metamorphic and magmatic events at Ledge Mountain. Zircon is a refractory mineral that can survive high-grade metamorphism, partial melting, and even more extensive magmatism which makes them well-suited for determining primary crystallization ages within metamorphosed igneous rocks (McLelland and Chiarenzelli 1990, from Silver 1969, p. 247). A greater understanding of the geologic history of Ledge Mountain migmatites can contribute to the Grenville Province by placing the timing of the exhumation of the deep crustal rocks at LM. and to granulite-facies metamorphism as a whole by interpreting cathodoluminescence textures in high-grade zircons.

The Grenville Province is a large hot orogen that underwent numerous orogenic events from 1245 to 1155 Ma followed by extensional collapse in ~1150 Ma (Chiarenzelli et al., 1988; McLelland et al., 1990; 1996; 2004; Rivers, 2008; 2012; 2015). The Adirondack Mountains in northeastern New York are a southern extension of the Grenville Province (Fig. 1; Chiarenzelli et al., 1988; McLelland et al., 1988; Rivers, 2008). The Adirondack Highlands are well-known for recording high-grade metamorphism from 1200-1160 Ma, and granulite-facies metamorphism from 1090-980 Ma (McLelland et al., 2010; Peak et al., 2018). More recently, ultrahigh-temperature (UHT) metamorphism has been reported for two localities in the Highlands – Gore Mountain, 25 km east of Ledge Mountain, (Shinevar et al., 2021) and Ledge Mountain (Metzger et al., 2022). Migmatites are high-grade granulite-facies rocks that reach super-solidus temperatures and begin to melt (Sawyer, 2008). These exhumed deep crustal rocks have undergone extensive investigation especially throughout the Adirondacks (Bickford et al., 2008; McLelland et al., 2013; Rivers, 2015). U-Pb geochronology studies in the Adirondacks have placed metamorphism in the central Highlands around ~1170 to 990 Ma (Chiarenzelli et al., 2017, Peak et al., 2018, Aleinikoff et al., 2021). Metzger et al. (2022) reported U-Pb zircon SHRIMP ages from Ledge Mountain migmatites of 1085 ± 13 Ma to 968 ± 5 Ma for recrystallized rims formed following UHT conditions during near-isothermal decompression on the retrograde cooling path metamorphic zircons. The youngest ages from Metzger et al. (2022) are c. 968 ± 5 Ma for pegmatitic leucosomes – that result from analyses of just 3 zircon grains – are much younger than previous dating and suggest migmatization continued into late past previous estimates of granulite facies metamorphism from 1090-980 Ma.

Previous work within the Highlands sets the pressure-temperature (P-T) conditions at 600°-850°C and 5-8 kbar (Bohlen et al., 1985; Florence and Spear, 1995; Spear and Markussen, 1997; Storm and Spear, 2005). These estimates are based on classical inverse thermobarometry (Lasalle and Indares, 2014) which can be problematic in high-grade metamorphic terranes due to post-peak diffusion and re-equilibration (Spear and Florence, 1992). Phase equilibria modeling has been underutilized in the Highlands (e.g., Metzger et al., 2022) and is better suited for high-grade terranes. Using phase equilibria modeling, Metzger et al. (2022) showed that Ledge Mountain migmatites are *ultra*high-temperature rocks with minimum peak conditions of 960-1025°C and 11-12.5 kbar. Ultra-high temperatures have also been identified at Gore Mountain where Shinevar et al. (2021) reported peak metamorphic PT conditions at 950 ± 40°C and 9-10 kbar. This has important implications for late- to post-orogenic crustal dynamics in Grenville province.

Metzger et al. (2022) used petrographic analysis to identify retrograde and former melt textures in Ledge Mountain zircons. They found evidence of isothermal decompression that was indicated by decompression textures including biotite symplectite and ilmenite-after-rutile relationships. They identified lobate quartz inclusions in garnet which were inferred to be a result of peritectic garnet growth during dehydration melting. Retrograde textures were identified as sericitized feldspar, chloritized biotite and corroded sillimanite, and the presence of garnet rims replaced by biotite-plagioclase-sillimanite intergrowths.

Extensive work has been done dating and reconstructing the events along the boundaries of the Adirondack Highlands, but there is less research in the central Highlands - Marcy Massif (Peck et al., 2018 and Regan et al., 2019), Gore Mountain (Shinevar et al., 2021) and Ledge Mountain (Metzger et al., 2022). An understanding of the high-grade metamorphism around the world contributes to our interpretations of the UHT metamorphism at Ledge Mountain. Further understanding of the timing of metamorphism at Ledge Mountain and analysis of these migmatites can help explain the tectonic setting of the Highlands. Large-scale collisional events will forever occur due to the ever moving tectonic plates. Today, the collision between India and Asia forming the Himalayan Mountains are the largest modern example of mountain building similar to the Grenville orogen. On a smaller scale, an understanding of the metamorphism at Ledge Mountain can further our understanding of larger tectonic events. Zircons preserve a metamorphic and melting history that plays a key role in piecing together a timeline of events and the mechanisms.

In 2021, I collected 19 samples from both western and eastern Ledge Mountain for further U-Pb geochronology analysis to constrain the timeline for metamorphism, anatexis, and migmatization. Metzger et al. (2022) recorded young rim recrystallization ages (1047 ± 5 to 1035

± 2 Ma) and inherited core ages (1136 ± 5 Ma). They proposed the gneiss dome as the mechanism for crustal exhumation but only recorded zircons that recrystallized after the exhumation. My work adds more U-Pb zircon SHRIMP results to better understand metamorphism and magmatism in the central Highlands by recording the timing of the actual exhumation events predating Metzger et al. (2022). Here, I present new U-Pb zircon SHRIMP geochronology, CL image analysis of zircon, trace element geochemistry, whole rock major and trace element geochemistry, and petrographic analysis of four samples (AD01, 17LM01, 17LM07, and 17LM14; Fig. 2) from western Ledge Mountain that were collected across multiple field seasons. Cathodoluminescence textural analysis, zircon trace element analysis suggests that these three samples of microscopically interlayered melanosome and leucosome and one sample of pegmatitic leucosome migmatites have undergone metamorphism both by recrystallization in the presence of anatectic melt and post anatexis. Cathodoluminescence imaging has revealed a range of textures within zircon domains suggesting different forms of metamorphism; including chaotic textures suggesting recrystallization in the presence of an anatectic melt from 1057 to 1045 Ma and homogeneous textures suggesting recrystallization after the anatexis from 1038 to 1022 Ma. These chaotic textures have not been previously identified at Ledge Mountain and give new insight to the timing of anatexis and exhumation.

GEOLOGIC BACKGROUND

The Grenville Province

The Grenville Province, which stretches from northeastern Canada to western Texas (Fig. 1b; Metzger et al., 2022), is a Mesoproterozoic orogenic belt that has experienced 4 major tectono-magmatic events over the span of more than 200 million years (McLelland et al., 1996; 2010; 2013; Rivers, 2012; 2015). The Grenville orogenic cycle includes the Elzevirian Orogeny, the Shawinigan Orogeny, anorthosite-charnockite-mangerite-granite (AMCG) magmatism, and the Grenvillian Orogeny, dating from around 1245-980 Ma (McLelland et al., 1996; 2010; 2013; Rivers, 2015). Rocks in the Grenville province range in age from Archean to Mesoproterozoic (McLelland et al., 2013, and Rivers, 2015)

The Elzevirian Orogeny, beginning 1245 Ma, was formed by the collision of supercontinent Laurentia and the Central Metasedimentary Belt back-arc basin beginning the formation of the Grenville Province (McLelland et al., 1996; 2010; 2013). The Shawinigan Orogeny, 1200-1160 Ma, resulted from the collision with Laurentia and Adirondis, another back-arc basin (McLelland et al., 2010; 2013). The Shawinigian orogenic event created the upper amphibolite-facies rocks in the Adirondack Lowlands and thrust the Lowlands over the Highlands along the Carthage-Colton shear zone (CCSZ) (McLelland et al., 2010; 2013).

The AMCG magmatism was an anorogenic event, ~1150, caused by the post-orogenic collapse and the delamination of over-thickened Shawinigan crust (McLelland et al., 2004; 2010; 2013). Delamination occurs when lithospheric mantle separates from the base of the crust, creating room for new, hot asthenosphere to flow in, and resulting in the AMCG intrusions (McLelland et al., 2010; 2013). Post-orogenic collapse is a foundational step in the orogenic process (Wong et al., 2012).

The Grenvillian Orogeny, subdivided into the Ottawan phase and the Rigolet phase, was the final deformational event in the Adirondack Highlands from 1090-980 Ma that resulted from the collision between Laurentia and Amazonia forming the supercontinent Rodinia (McLelland et al., 2010; Rivers, 2009). The Ottawan phase created a 60-80 km thick plateau that overprinted the Shawinigan metamorphism in the Highlands (McLelland et al., 2013). There was late Grenville extension along the CCSZ and the East Adirondack Shear Zone (EASZ) (Fig. 1a, McLelland et al., 2013; Chiarenzelli et al., 2017; Metzger et al., 2022). This long series of large scale orogenies, high-grade granulite-facies metamorphism, deformation, and anatexis created the Grenville province.

The Adirondack Highlands

The Adirondack Mountains are a southern extension of the Grenville Province in upstate New York (Fig. 1a). The Adirondack Mountains are an uplifted, domal exposure of mesoproterozoic high-grade gneiss. The Adirondacks are divided into the Lowlands (LL) and the Highlands (HL) which are separated by the CCSZ (Fig. 1a).

The Lowlands are carbonates and siliciclastics sediments that metamorphosed into upper amphibolite-facies metasedimentary rocks (Streepey et al., 2001). The Adirondack Highlands are granulite-facies plutonic rocks (McLelland et al., 2010; 2013). The Lowlands are 100 Ma older than the Highlands (Streepey et al., 2001). The Lowlands, known as the orogenic lid, overlaid the Highlands prior to the Ottawan and later motion moved them to their current position (Rivers, 2012). Structural features of the Lowlands and the Highlands date during the Shawinigan and Ottawan. The higher topography of the Highlands relative to the Lowlands is due to the more erosion resistant composition of the granulite facies rocks of the Highlands compared to the metasedimentary rocks of the Lowlands. Streepey et al. (2001) says that post-orogenic extension dropped the Lowlands and raised the Highlands.

The CCSZ is a normal fault that dips 45° to the northwest, 1–15 km-wide, along the boundary of the HL and LL. The CCSZ is a zone of deformation (Hamilton et al., 2004 and Selleck et al., 2005,). Shearing and deformation within the CCSZ occurred from 1120-1080 Ma (Grant et al., 1986 in McLelland et al., 1988; Hamilton et al., 2004; and Selleck et al., 2005), the range of CCSZ movement. Deformed/mylonitic granite was emplaced during the active shearing of the CCSZ. Selleck et al. (2005) confined the timing of granite emplacement in the CCSZ.

Uranium-lead (U-Pb) geochronologic analysis has been conducted on zircons from the CCSZ. Zircons from granite pegmatite mylonitized on its margins dated 1044 ± 7 Ma were interpreted as intruding during normal strain (Selleck et al., 2005). Penetrative deformation from shearing with 1195 ± 11 zircon cores and 1035 ± 10 zoned zircon rims (Selleck et al., 2005). Lyon Mountain granite was emplaced from 1045 to 1037 Ma (Selleck et al., 2005). The Diana Complex unit is a mafic syenite gneiss located along the southern CCSZ (Selleck et al., 2005; Hamilton et al., 2004; and Baird, 2020). Zircon rims interpreted as a metamorphic event are 1122 ± 29 Ma and zircon cores indicating the timing of emplacement are 1164 ± 11 Ma (Hamilton et al., 2004). U-Pb geochronology analysis has also been conducted on titanite from the CCSZ. These ranges of granite emplacement ages (1045-1037 Ma) and deformation (1181-1122 Ma) in the CCSZ occurred during the exhumation of the high-grade rocks Highlands.

The Piseco Lake shear zone (PLSZ), a lithotectonic discontinuity, separates the Central Highlands from the Southern Highlands which are inferred to have had different geologic histories (Valentino et al., 2018; Fig 1A). Granitoids from the PLSZ were emplaced from 1205 to 1180 Ma (Valentino et al., 2018).

The Highlands are a proposed gneiss dome; extension along the CCSZ and the East Adirondack shear zone (EASZ), possibly correlated to the Tawachiche shear zone (Fig. 1A) are potential mechanisms for this gneiss dome (Bickford et al., 2008; Wong et al., 2012; Regan et al., 2019; Metzger et al., 2022). The synextension of the CCSZ contributed to exhumation of the high-grade rocks of the Highlands.

The felsic Anorthosite-Mangerite-Charnockite-Gneiss (AMCG) Suite is also found in the Highlands and makes up the Marcy Massif, Oregon Dome, and Snowy Mountain dome (Fig. 1a), for example. Wong et al. (2012) dated zircons from granitic gneiss with an age of 1145-1140 Ma, coeval with AMCG magmatism.

Hawkeye Granite Gneiss and Lyon Mountain Granite Gneiss are found in the Highlands (Fig. 1a). Very deformed Hawkeye Granite Gneiss was intruded by the weakly deformed Lyon Mountain Granite Gneiss. Aleinikoff et al. (2021) recently used U-Pb SHRIMP analysis to conclude that the Hawkeye granite gneiss was emplaced from 1160 to 1155 Ma and Lyon Mountain granite gneiss zircon cores set the timing of igneous emplacement from 1150-1145 Ma. Placing both Hawkeye Granite Gneiss and Lyon Mountain Granite Gneiss as late members of the mangerite-charnockite-granite suite. The metamorphic zircon rims were dated from multiple metamorphic events ranging from 1080-990 Ma, during the Ottawan.

The Marcy Massif is an anorthosite pluton that dominates the HL (Fig. 1a). Numerous researchers have conducted U-Pb geochronology analysis of zircons from the Marcy Massif. Peck et al. (2018) dated in-situ zircons from anorthosite in the Marcy Massif and interpreted the age of metamorphic mineral growth in the Adirondack anorthosite at 1050-1035 Ma and an older crystallization age of pluton from 1180 Ma to 1125 Ma. An in-situ zircon from a ferrodiorite gneiss was dated 1051 ± 24 Ma. McLelland and Chiarenzelli (1990) U-Pb dated zircons from

Marcy Massif anorthosite and found a minimum age of anorthosite intrusion at 1113 Ma and estimated the igneous crystallization from 1135-1125 Ma. Regan et al. (2019) used U-Th-Pb geochronology of monazites to date the Marcy Massif from 1050 to 980 Ma interpreted as fluid-mediated dissolution reprecipitation, rocks cooled isobarically after accretionary orogenesis and emplacement of the AMG. Regan et al. (2019) used U-Th-Pb geochronology of monazite to conclude that deformation around and over the Marcy Massif occurred from 1070 to 1060 Ma. An inherited core from a granitoid was 1230 Ma. The Marcy Massif was a zone of high pressure (7-8 kbar) and high temperature (~800-850°C) metamorphism (Spear and Markussen, 1997).

Gore Mountain is located in the central Highlands, 35 km south of the Marcy Massif (Fig. 1a) and 25 km east of Ledge Mountain (LM). Shinevar et al. (2021) used thermobarometry, thermodynamic modeling, and diffusion modeling of Gore Mountain garnet amphibolites to estimate UHT P-T conditions (9-10 kbar, 950 ± 40°C) at 1053.9 ± 5.4 Ma (MSWD=0.94). Hamilton et al. (2004) used U-Pb ages of zircon from Gore Mountain charnockite to date 1041 ± 6 Ma. Snowy Mountain is an anorthosite dome located in the central Highlands, 5 km southwest of Ledge Mountain, and experienced granulite facies metamorphism at 1031 ± 30 Ma (Hamilton et al., 2004). Oregon dome is 30 km southeast of LM and experienced granulite facies metamorphism at 1048 ± 10 Ma (Hamilton et al., 2004). The Marcy Massif and Gore Mountain are both areas of high temp metamorphism within the Highlands. The most recent evidence of UHT metamorphism in the Highlands was found at Ledge Mountain (Metzger et al., 2022).

Ledge Mountain

Ledge Mountain is located in the central Adirondack Highlands (Fig. 1a) and is an area of high-grade metamorphism, anatexis (partial melting), and migmatization. Ledge Mountain, along with Snowy Mountain and the Oregon anorthosite massifs, are part of a proposed gneiss dome that helps to explain the exhumation of these deep crustal rocks (Bickford et al., 2008; McLelland and Selleck, 2011; Wong et al., 2012; Regan et al., 2019; Metzger et al., 2022). Gneiss domes are a common feature in late- to post-orogenic belts that result from extension and exhumation of high-grade rocks – often cored and buoyed by granites – after orogenesis (Teyssier and Whitney, 2002). Ledge Mountain migmatites are in the core of a recumbent antiform and bordered to the north and south by marble (Geraghty, 1978). Based on the U-Pb zircon geochronology in Metzger et al. (2022), exhumation of this gneiss dome would have taken place in the late- to post-Ottawan phase (~1050 Ma).

Ledge Mountain felsic migmatites form a boomerang-shaped mountain with a steep southern face (Fig. 2). Metzger et al. (2022) found that migmatites from western Ledge Mountain had UHT metamorphic P-T conditions of 960-1025°C and 11-12.5 kbar based on petrographic microtextures, mineral compositions, and phase equilibria modeling; these results yielded significantly higher P-T conditions than previous studies of high-grade rocks from the Adirondack Highlands. Estimated metamorphic *P-T* conditions for other granulite-facies rocks from around the Highlands based on classic mineral thermobarometry including two-feldspar; Fe-Ti oxide solvus; and Fe-Mg exchange thermometry for orthopyroxene- clinopyroxene; garnet-biotite; and garnet- pyroxene pairs; and garnet-aluminosilicate-silica- plagioclase (GASP) and other barometers span 600–850 °C and 6–8 kbar (e.g., Bohlen and Essene, 1977; Bohlen et al., 1980, 1985; Florence and Spear, 1995; Spear and Markussen, 1997; Storm and Spear, 2005; McLelland et al., 2013). Ultrahigh-temperature granulites are an exciting discovery because they imply that the earth's crust is capable of experiencing and tolerating extreme thermal conditions on a regional scale (Harley, 2004, cit. in Kelsey et al., 2008).

Metzger et al. (2022) completed U-Pb zircon SHRIMP geochronology for ten melanosome and leucosome samples from migmatites (see the migmatite section following this section for definitions) and found Ottawan to post-Ottawan metamorphism and anatexis from 1085 ± 13 to 959 ± 14 Ma. Metzger et al. (2022) concludes that the metamorphic zircon rims give a mean age of 1047.0 ± 4.6 Ma likely recording recrystallization at granulite-facies conditions post-peak UHT conditions and on the retrograde path. The mean age of crystallization from melanosomes of 1035.2 ± 2.4 Ma may represent dissolution and/or recrystallization after extraction of leucocratic melts Metzger et al. (2002) interpreted this to indicate a prolonged period of metamorphism during the Ottawan.

Migmatites

Ledge Mountain migmatites are characteristic sillimanite-bearing granulite-facies metamorphic rocks in the Adirondack Highlands region (McLelland et al., 1996; 2010; 2013; Rivers, 2015). A migmatite is a mixed metamorphic and igneous rock that is composed of two parts, one formed by partial melting, the *neosome*, and one unaffected by partial melting, the *paleosome*. Structures in the paleosome are preserved from the original parent rock (Sawyer, 2008). The partial melting process, called anatexis, occurs when an input of heat increases temperatures until melting begins; melt can begin to migrate when the rock becomes permeable and has reached a minimum percentage of melt (less than 2 vol%; Sawyer, 2008). Partial melting in continental crust is often associated with tectonic deformation, like what is seen in the Adirondacks or in the core of the modern Himalaya. The segregation and migration in migmatites is likely from differential stress.

The paleosome represents the parent rock. The neosome has two parts: *melanosome* and *leucosome*, that are classified separately from each other by mineralogy, structure (foliation, folds, and layering), and microstructure (shape, size, and orientation of grains) (Sawyer, 2008). The melanosome is a darker, more mafic part of the rock that is left unmelted during anatexis. Ledge Mountain melanosomes are predominantly quartz, feldspar, and plagioclase with sillimanite, garnet, biotite, and Fe-Ti oxide minerals. The leucosome is lighter in color and formed in-situ during anatexis. Ledge Mountain leucosomes are predominantly quartz and k-feldspar. Some leucosomes coarse texture of quartz and K-feldspar are referred to as pegmatitic leucosomes. The migmatites at Ledge Mountain vary from melanosome, interlayered melanosome and leucosome, and pegmatitic leucosome (Fig. 3). Sample 17LM01 is a pegmatitic leucosome. Samples 17LM07, 17LM14, and AD01 are microscopically interlayered melanosome and leucosome.

These migmatites contain zircons which are key to U-Pb geochronology and petrographic analysis of textures and zoning. Zircons have a unique ability to survive magmatic, metamorphic, and erosional events and preserve structures from such events (Corfu et al., 2003). Two distinct cathodoluminescence textures have been identified in Ledge Mountain zircons; homogeneous and chaotic textures. Notably, dated zircon domains of chaotic textures suggest recrystallization in the presence of the anatectic melt that resulted in the exhumation of the central Highland gneiss dome. Zircons were used for U-Pb geochronology, trace element chemistry, and petrographic analysis that help frame the anatectic history of these rocks.

SAMPLE SELECTION, ANALYTICAL METHODS & RESULTS

I completed three weeks of field research in August-September 2021 during which I mapped the central part of the Rock Lake quadrangle north of Indian Lake, NY, and collected 19 samples from both western and eastern Ledge Mountain for further U-Pb zircon geochronology, geochemistry, and petrography. Forest coverage is heavy and rock outcrop exposure is limited in the Ledge Mountain region (see outcrops marked on Fig. 2, Field photos in Fig. 3). Exposed outcrops were often very weathered and made for poor samples. I focused on collecting as many samples as possible while also covering as much area as possible. Field work was supported by a U.S. Geological Survey EDMAP grant, and I submitted a final 1:12,000-scale geologic map of the area in November 2022 (Fig. 2; Appendix I). I selected four migmatite samples; three melanosome with microscopically interlayered leucosome (AD01, 17LM07, 17LM14) and one pegmatitic leucosome (17LM01) (Table 1; Fig. 2; see sample descriptions below) collected from western Ledge Mountain for zircon separation, and U-Pb zircon SHRIMP geochronology and trace element analysis. Below I describe the petrography of these four samples.

Sample Descriptions & Petrography

Ledge Mountain migmatites are described by their mineralogy and textural heterogeneity on a microscope to outcrop scale. I studied macro- and micro-textures using a petrographic microscope to understand the metamorphic and partial melting histories at Ledge Mountain. The migmatites are mostly homogenous in regards to mineralogy and texture except for pegmatitic leucosomes which are much coarser than typical leucosome. Photomicrographs showing macro- and micro-textures are shown in Figure 4.

The four sampled rocks all have many features and mineral assemblages in common. I will describe the common features found in all of the sampled rocks and then later describe each rock individually. The primary mineral assemblage includes quartz and feldspar in varying proportions of quartz, alkali feldspar, and plagioclase. Additionally, biotite, Fe-Ti oxides (ilmenite and/or magnetite), sillimanite, and muscovite are often present. Accessory minerals include hercynite and zircons. Lenses made of sillimanite and quartz are found in some samples. Grains range from fine to coarse grained. Foliation can be defined by an alignment of sillimanite grains. In some samples, distinct contacts between melanosome and leucosome are found.

Garnet is scarce, poikiloblastic, and heterogeneously distributed; grains vary in size from 1 to 5 mm and occur as larger peritectic grains, relict garnets, and small scattered crystals (Fig. 4a and 4b). Garnet is found in AD01 and 17LM07. Larger garnets are peritectic and include inclusions and embayments of quartz, plagioclase, feldspar, biotite, and/or Fe-Ti oxides (Ilmenite and/or magnetite). Peritectic garnets grow in the presence of melt. Garnets include both monomineralic and polymineralic inclusions. (Fig. 4a and 4b). Garnet is a high-temperature and high-pressure mineral.

Quartz inclusions are rounded. Biotite and Fe-Ti oxides are often found/seen grown together. Feldspar is often found as melt rims along grain boundaries (Fig. 4b). Sericitized feldspar is common. Sillimanite is the only aluminosilicate I have identified. It is found as acicular grains in lenses (fibrolite) and/or as blocky grains, and often aligned. Myrmekite is common (sign of decompression texture). Sericitization of plagioclase is common. Biotite is common. Higher biotite percentages are found in the melanosome. Biotite is often found in association with Fe-Ti oxides, often replacing oxide minerals. Chloritized biotite is found in some samples (retrogression/overprinting). Biotite is found as inclusions in garnet and filling in cracks/as fluid inclusions in garnets. Biotite found as melt films are grain boundaries. Chlorite is common and can be found chloritizing biotite. Fe-Ti oxides (ilmenite and/or magnetite) are common and are found as inclusions and embayments in garnets, intergrown with biotite, being replaced by biotite, alongside sillimanite, and as isolated minerals. Hercynite is always found in association with Fe-Ti oxides.

Zircon is found in the leucosome and melanosome. Grains are small (micron scale) with pleochroic halos (can be monazite or apatite as well). Grains are rounded, subhedral, to elongated. Zircons are found in the matrix and included within opaques, plagioclase, and sericitized feldspar. In crossed polarized light, two domains can be found in zircons. They appear as a core within a zircon or as a growth halo around the grain.

Melanosomes are usually granoblastic to weakly foliated, higher concentrations of biotite, myrmekite, microcline, quartz, sercite. The quartz and feldspar in melanosome domains are fairly coarse and are all found in the melanosome. Fe-Ti oxides are also present in the melanosome.

Leucosome is usually 1-2 % biotite, mostly quartz and feldspar (can be plagioclase and/or microcline), and often has sillimanite, garnet, hercynite, opaques (Fe-Ti oxides). There is an alignment of minerals, predominantly exhibited in the sillimanite but also found with the biotite and Fe-Ti oxides, in the microscopically interlayered leucosome. Pegmatitic leucosomes are coarser comparatively and will be mostly quartz and feldspar.

Evidence for the Former Presence of Melt

Textural evidence signifies crystallization in the presence of former melt is common throughout migmatite samples. (1) Rounded to lobate quartz and nanogranite inclusions in garnet that are inferred to be a result of peritectic garnet growth during dehydration melting (Fig. 4); (2)

Inclusions of opaques, biotite, chloritized biotite, muscovite and feldspar; (3) String of beads of quartz are evidence of melt along a former grain; (4) Melt films in the form of feldspar, opaques, and biotite along grain boundaries and Fsp around Fe-Ti oxide grains; (5) Microcline as melt films along grain boundaries and as embayments; (6) Euhedral faces next to former melt; (7) Muscovite filling in fractures; (8) Lobate opaques (appear to fill in during melt). Textural evidence of retrogression includes (1) sericitized feldspars, (2) retrograde biotite, chloritization of biotite, and (3) the small presence of muscovite.

Rock Descriptions

I describe each of the dated rocks in detail below with abbreviations from Whitney and Evans (2010):

AD01 – 43°48’38”N, 74 18’32”W

AD01 was collected from the west-most edge of Ledge Mountain (Fig. 2). This rock is a migmatite with microscopically interlayered melanosome and leucosome. Sillimanite is moderately aligned and there is compositional banding between melanosome and leucosome in the sample. In hand sample, AD01 is fine- to coarse-grained, with Qz, Fsp, Bt, and rich in Grt. Twenty-nine zircons were analyzed for U-Pb geochronology from this sample. Zircon grains are rounded, subhedral, to elongate and found in the melanosome and leucosome. The mineral assemblage includes: *Qz + Pl + Ksp + Bt + Grt + Sil + Ms + Chl + (Rt + Ilm + Zrn + Mag ± Hc ± Ap ± Mnz) + Opaques + Myrmekite (trace)* (Table 1)

17LM01 – 43 48’39”N, 74 18’45”W

17LM01 was collected from the west most edge of Ledge Mountain close to the “knob” visible from the topography (Fig. 2). 17LM01 is a pegmatitic leucosome. There is no foliation present in the one thin section of this rock. In hand sample, 17LM01 is fine to coarse grained, with quartz, plagioclase, feldspar, and biotite visible. Thirty-two analyses from 30 zircon grains were analyzed for U-Pb geochronology from this sample. Zircons grains are rounded, subhedral, to elongate grains and are found in the pegmatitic leucosome included in plagioclase, opaques, sericitized feldspar. Some cores are found within the zircon grains. Muscovite found overprinting an opaque. The mineral assemblage includes: *Qz + Ksp/Mc + Pl + Bt + Ms + opaques (Fe-Ti oxides) + Zrn + Chl + Sil ± Rt* (Table 1, Abbreviations from Whitney and Evans, 2010)

17LM07 – 43 48’38.1”N, 74 18’31.9”W

17LM07 was collected along the west most edge of Ledge Mountain (Fig 2). 17LM07 is a fine to coarse grained, microscopically interlayered pegmatitic leucosome and melanosome. Leucosome and pegmatitic leucosome had no distinct foliation or flow banding present but sillimanite is aligned. Twenty zircons were analyzed for U-Pb geochronology from this sample. Zircons are present throughout the microscopically interlayered leucosome and melanosome in both the melanosome and the leucosome. Zircon grains are rounded, subhedral, to elongate and found in the matrix and inclusions in an opaque and in feldspar. The mineral assemblage includes: *Qz + Ksp + Pl + Mc + Sil + Grt + Bt + opaques (Fe-Ti Oxides) + myrmekite + OPX + Ser + Zrn + Ms ± Chl + Hc* (Table 1, Abbreviations from Whitney and Evans, 2010).

17LM14 – 43 48’35.2”N, 74 18’19.8”W

17LM14 was collected from the southeastern slope of the western branch of Ledge Mountain (Fig. 2). 17LM14 is a fine to coarse grained, microscopically interlayered melanosome and leucosome with rounded to irregular shaped grains that range in diameter from 0.5 to 1.5 mm. Twenty-two analyses from 20 zircon grains were analyzed for U-Pb geochronology from this sample. Zircons are rounded to elongate, 0.05 mm in diameter and are found in the melanosome associated with plagioclase, quartz, and opaques. No foliation is found in thin sections of

17LM14. Zircons are present in the matrix. Zircon grains are rounded, subhedral, to elongate and found in the melanosome. The mineral assemblage: *Pl + Ksp/Mc + Qz + Bt + Opq (Fe-Ti oxides) + Myrmekite + Zrn + Ms + Chl + Sil* (Table 1, Abbreviations from Whitney and Evans, 2010).

Whole-Rock Geochemistry

The four samples were analyzed for whole rock geochemistry by x-ray fluorescence (major elements) and inductively coupled plasma mass spectrometry (ICP-MS) (trace elements) at the GeoAnalytical Lab at Washington State University (Pullman, Washington, USA) (Table 2, Figs. 5 and 6). Whole rock major and trace element analyses for the four migmatite samples used for discrimination diagrams are summarized in Table 2 and plotted in Figures 5 and 6, analyses from Metzger et al. (2022) are included for comparison.

<u>Major Element Characteristics</u>

Three of the analyzed Ledge Mountain migmatite samples have granitic compositions and one plots in the tonalitic field. Three of the four samples plot as granite on an Ab-An-Or diagram (Ab-Albite, An-Anorthosite, Or-Orthoclase; Fig. 5a). All four samples have a limited range of SiO_2 (69.48 - 71.73 wt%) (Fig. 5d, Table 2). They are generally potassium rich (K_2O = 2.88 - 6.47 wt% and 1 analysis at 1.42 wt%) and are strongly peraluminous (A/CKN >1.1 [molecular ratio of $Al_2O_3/(CaO+NaO_2+K_2O)$]; Fig. 5b, Table 2), range from alkali calcic to calcic (Fig. 5c) and are generally ferroan [FeO/(FeO+MgO)=Fe*] with one analysis magnesian close to ferroan, according to the terminology of Frost and Frost (2008; Fig. 5d).

<u>Trace Element Characteristics</u>

Chondrite-normalized whole rock rare-earth element (REE) patterns for Ledge Mountain migmatites are plotted in Figure 6a. All four samples show a negative slope in the LREE

(Sm/La_N ratio ranges from 0.35 to 0.39; N - normalized; Light rare-earth element) and a negative anomaly for Eu ($Eu/Eu^* = Eu_N/ (Sm_N \times Gd_N)^{0.5}$; ranges from 0.54 to 0.64). Sample AD01 is separated as AD01a, AD01b, and AD01b Replicate fb (Table 2). AD01b and AD01b replicate fb were averaged to create one analysis for AD01b. Sample AD01a, AD01b, and 17LM01 have a flat slope in the HREE (Lu/Gd ratio; 0.70, 0.65, and 0.92 respectively). Sample 17LM14 has a weakly negative slope in the HREE (Lu/Gd ratio; 0.49). Sample 17LM07 has a positive slope in the HREE (Lu/Gd ratio; 3.00; Heavy rare-earth element), enriched in HREE. Metzger et al. (2022) LM samples and Lyon Mountain Granite samples were plotted comparatively. The patterns are similar with the negative slope of the LREE, the Eu depletion, and the nearly flat to weakly negative HREE slope. One Metzger meta-leucotonalite sample 11 has a positive HREE slope comparable to 17LM07. LM migmatite samples plot in the A-type granite field on the Zr versus 10^4 x Gallium/Aluminum (Ga/Al) diagram of Whalen et al. (1987; Figure 6b) and in the within-plate granite field on the Rubidium versus Yttrium + Niobium (Rb versus Y+Nb) diagram of Pearce et al. (1984; Fig. 6c).

Zircon Descriptions, Cathodoluminescence Imaging, and U-Pb SHRIMP Results

Zircons from the four samples were analyzed for trace element geochemistry and Uranium-lead (U-Pb) geochronology at the Stanford-U.S. Geological Survey (USGS) SHRIMP-RG Lab (RG is reverse geometry); data is on Table 4. Zircon rare earth element (REE) data for zircons from each of the four migmatite samples are normalized to C1 carbonaceous chondrite McDonough and Sun (1995, in Table 2, Column 1 “This study”) and plotted on $\log_{10}$ versus element plots on Figure 7a. Figure 7b shows my zircon REE data compared to other UHT and metamorphic zircons which will be discussed later in the discussion section of this thesis. Zircon grains were mounted in indium, polished, and imaged using cathodoluminescence (CL), backscattered electron (BSE) and scanning electron (SEM) microscopy to identify internal structure, inclusions, and physical defects. Isoplot-R from Santa Barbara is used to create weighted mean age histograms and U-Pb concordia diagrams (Fig. 9). Zircon ^{207}Pb corrected vs ^{206}Pb/^{238}U ages and ^{204}Pb corrected ^{238}U/^{206}Pb and ^{204}Pb corrected ^{207}Pb/^{206}Pb were plotted. U-Pb analysis locations were focused on outer domains to try to capture metamorphic and anatectic zircon and to look for younger ages like the Rigolet ages found in Metzger et al., 2022.

A total of 99 zircon grains from the four rock samples were dated using the SHRIMP with a total of 103 analyses. Twenty-nine spots were analyzed on 29 zircon grains from AD01. Thirty-two spots were analyzed on 30 zircons from 17LM01. Twenty spots were analyzed on 20 zircons from 17LM07. Twenty-two spots were analyzed on 20 zircon grains from 17LM14. The CL textures were compared to the U-Pb SHRIMP ages to make interpretations on which textures were dated. All grains were imaged on the JEOL JSM-IT500HR scanning electron microscope, equipped with a Centaurus monochromatic CL detector at Stanford University. Grains were analyzed for grain morphology, internal patterns (oscillatory zoning, chaotic zoning, etc.), zircon domains, and domain morphology. All zircons from each rock sample are pictured in Appendix III.

Zircon external morphology was analyzed for all grains. Aspect ratios were calculated for grains, elongated grains are described as any grain with an aspect ratio of ≥ 1:3. Zircon grains are rounded, subhedral, to elongate.

Zircon growth domains are defined by core, mantle, and rims (Corfu et al., 2003). I identified these domains within each grain. Not all grains have/retain all three domains. All my grains only have a rim and core domain, except for one grain, 17LM01-30.1 which has a rim, core, and an inherited core (Fig. 10A). Rims are the youngest part of a zircon grain since they grew or underwent alteration most recently. My rims are usually thin, follow the shape of the grain, and are dark in CL. Metzger et al. (2022) dated rims from western LM migmatites and found near concordant ages of rims from interlayered leucosome and melanosome ranging from 1067 ± 8 to 1006 ± 24 Ma, rims from leucosomes ranging from 1085 ± 13 to 959 ± 14 Ma, and rims from melanosome adjacent to leucosome from 1064 ± 9 to 972 ± 10 Ma. Mantles are transitional domains between rims and cores and have self-explanatory age differences between the rim and core. Metzger et al. (2022) dated mantles from Western LM migmatites and found near concordant ages from a melanosome with interlayered leucosome of 1097 ± 29 Ma, from pegmatitic leucosome samples ranging from 1152 ± 13 to 1070 ± 20 Ma, and from a melanosome adjacent to pegmatitic leucosome ranging from 1052 ± 8 Ma. Cores are the oldest part of a zircon grain and preserve the magmatic growth of the grain. My cores are usually rounded to subhedral, with CL characters of variable textures and brightness ranging from bright to dark. My cores from the four samples range from ~1045 to 1036 Ma (weight mean ages, Table 4, Fig. 9). Metzger et al. (2022) dated near concordant ages of cores from a melanosome with interlayered leucosome with an age of 1101 ± 23 Ma, and from melanosome adjacent to pegmatitic leucosome ranging from 1195 ± 21 to 1107 ± 12 Ma with one analysis at 1027 ± 18 Ma. U/Pb ages are taken from the core domains of the zircons. Inherited/xenocrystic cores are older, preserving the original zircon forming event. Xenocrystic cores can be identified by the abrupt change in zoning or CL.

CL is distinguished by varying brightnesses ranging from bright to dark which I've classified using a gray scale. "Bright" looks nearly white to light gray in color, "medium bright" appears as a range of gray, and "dark" appears dark gray, nearly black, to black in color. I have classified CL textures into two traits: homogenous and chaotic. Homogeneous cores are nearly one consistent brightness and are usually medium bright in CL (see Fig. 10B for examples of homogeneous textures). The zircon rim domains are all homogenous with dark CL throughout (see AD01-16.1 for an example of a dark rim in Fig. 10B). Chaotic zoning ranges in CL character from bright to dark and follows no rhyme or reason, hence the name (see Fig. 10C for examples of chaotic textures). Chaotic zoning is found in the core domains of the sampled zircons. Chaotic textures in CL are common characteristics in zircons from granulite-facies rocks (Corfu et al., 2003). Oscillatory zoning patterns (OZP) are common zircon growth textures; they represent the heterogeneous distribution of trace elements (Hoskin, 2000). OZP appears as thin, banded, alternating bright and dark stripes, reminiscent of tree rings. Faded OZP is the degraded or blurred banding that shows thicker stripes with varying CL brightness, following the domain shape (see Fig. 10D for examples of faded OZP). Faded OZP is usually seen along the boundaries of the core domain and not throughout the whole domain. Homogeneous zoning, chaotic zoning, and/or faded OZP is found in the core domains.

Fractures are commonly found in the core domains across the length and along the length of the grain. CL brightness varies along fractures on some of the grains, see 17LM14-19.1 in Fig. 10A. Embayments (evidence of dissolution) are often found on the grain boundary and on the rim/core boundary, see 17LM07-4.1 in Fig. 10B. Inclusions may be found in some of the zircon grains. They look like spots of dark CL but without further analysis we are not able to conclude that all are inclusions. 17LM01-15.1's U-Pb SHRIMP age was taken from one of these dark spots, the age is discordant which leads us to believe this is an inclusion and not a zircon (Table 4, Appendix III).

AD01 (WMA = 1045.7 ± 0.1 Ma) (Fig. 9a, Table 4)

Most of the grains have a rounded (AD01-1.1), subhedral (AD01-17.1) to elongate (AD01-8.1) grain shape. Fractures are uncommon. Evidence of dissolution in the form of embayment is visible along the rim/core boundary and along the grain boundary on many grains (17LM01-3.1). There appear to be no inclusions in AD01 zircons. Only rim and core domains are found in AD01 zircons. AD01 rims are homogenous, dark in CL character, and show no texture or zoning patterns (AD01-16.1; Fig. 10B). Rims may follow the full grain shape (AD01-1.1) or are discontinuous around the grain (AD01-10.1). Cores have bright to dark CL with homogenous and/or chaotic textures. Faded OZP is found in a few of the AD01 cores.

Twenty-nine zircons were dated from sample AD01. All U/Pb ages for AD01 are taken from the core domain. Dates for concordant or near-concordant zircon cores from sample AD01 range from 1118.2 ± 21.1 to 930.2 ± 7.5 Ma with a weighted mean age of 1045.68 ± 0.13 Ma (Table 4; Fig. 9a). Two grains were excluded from weighted mean age estimates; AD01-2.1 (660.3 ± 11.7 Ma) was excluded because it has high Fe content (Table 3), is discordant (Fig. 9a), and an anomalously young age and AD01-24.1 (891.36 ± 15.0 Ma) was excluded because it is discordant (Fig. 9a) and has an anomalously young age. Zircons gave Th/U ratios of 0.00467 to 0.01959 for all the cores. See the Zircon Trace Element section below for AD01's REE and trace element analysis (Fig. 7A-a and 8). There are two populations of zircon ages; two grains AD01-27.1 and AD01-20.1 are significantly older and have a weighted mean age of 1083 Ma ±0.65%. Both of these grains have a chaotic domain. In the younger population, zircons displaying a chaotic domain in the core domain have a weighted mean age of 1056.0 ± 0.2 Ma and zircons homogenous domains have a weighted mean age of 1037.78 ± 0.17 Ma.

<u>17LM01 (WMA = 1036.9 ± 0.2 Ma) (Fig. 9, Table 4)</u>

Most of the grains have a subhedral (17LM01-14.1) to elongate (17LM01-10.1) shape. A few grains have a more rounded grain shape (17LM01-25.1). Fracturing and evidence of dissolution (17LM01-21.1) are common in 17LM01 grains. Evidence of dissolution is visible along the rim/core boundary and along the grain boundary on many grains (17LM01-29.1). There are some areas of dark CL that may or may not be inclusions but only 17LM01-15.1 can confidently be defined as an inclusion. 17LM01-30.1 is the only grain where rim, core, and an inherited core domain are visible/distinguishable (Fig. 10A). The inherited core has a medium bright CL with chaotic zoning. For all other zircons, only rims and/or cores were identified. Rims are rounded to subhedral, following the grain shape (17LM01-10.1), or may be negligible (17LM01-13.1). Rims are thin, homogenous, and dark in CL. Cores are rounded to euhedral, have bright to dark CL with homogenous and/or chaotic. CL brightness alteration along fractures in the core can be found (17LM01-13.1). Faded OZP is found in all grains (see 17LM01-29.1 for faded OZP; Fig. 10D).

Thirty zircon grains were dated from sample 17LM01 with 32 analyses. All U-Pb ages were taken from the core domains. Dates for concordant or near-concordant zircon cores from sample 17LM01 range from 1074.1 ± 6.9 to 930.2 ± 34.1 Ma with a weighted mean age of 1036.9 ± 0.2 Ma (Table 3; Fig. 9b). Zircon 17LM01-15.1 was excluded from weighted mean age estimates. Spot 17LM01-15.1 SHRIMP analysis was taken from a rounded area of medium bright CL within the core domain of the grain but the age is significantly young (855.9 ± 40.7 Ma; Fig. 9b) and has higher LREE concentrations (La, Ce, Nd; Table 3; Fig. 7A-b) and a weakly positive Eu anomaly (Fig. 7A-b). This does not make geologic sense that a core from this region would be so young; it is likely an inclusion within the zircon and therefore the age is disregarded. Zircons gave Th/U ratios of 0.0011 to 0.0417 for all the cores. See the Zircon Trace Element section below for 17LM01's REE and trace element analysis (Fig. 7A-a and 8). Zircons with chaotic domains have a weighted mean age of 1045.5 ± 0.27 Ma. Zircons with homogenous domains have a weighted mean age of 1032.16 ± 0.2 Ma.

17LM07 (WMA = 1037.6 ± 0.2 Ma) (Fig. 9, Table 4)

Most of the grains have a rounded to irregular (and broken grains) grain shape (17LM07-1.1). A few have a subhedral grain shape (17LM07-5.1). Fractures across the grain and embayments along rim/core and grain boundaries are common. There appear to be no inclusions in 17LM07 zircons. Only rim and core domains are found in 17LM07 zircons. 17LM07 rims are rounded to subhedral, following the grain shape (17LM07-4.1), and are thin, homogenous, and dark in CL. 17LM07 cores are medium bright to dark, and all are nearly homogeneous (17LM07-2.1). Faded OZP is found in all 17LM07 cores (17LM07-16.1 in Fig. 10D).

Twenty zircon grains were analyzed from sample 17LM07. All U-Pb ages for 17LM07 are taken from the core domain. Dates for concordant or near-concordant zircon cores from sample 17LM07 range from 1049.7 ± 14.5 to 994.7 ± 6.2 Ma with a weighted mean age of 1037.6 ± 0.2 Ma (Table 3; Fig. 9c). Two grains were excluded from weighted mean age estimates; 17LM07-9.1 (958.6 ± 5.8 Ma) is discordant and has relatively high Hf concentrations and 17LM07-12.1 (1029.0 ± 13.2 Ma) is discordant and has high Ti and Fe concentrations (Fig. 9c; Table 3 and Table 4). Zircons gave Th/U ratios of 0.01055 to 0.02907 for all the cores. See the Zircon Trace Element section below for 17LM07's REE and trace element analysis (Fig. 7A-c and 8c). All 17LM07 inner domains feature homogeneous textures and have a weighted mean age of 1037.6 ± 0.2 Ma.

17LM14 (WMA = 1045.2 ± 0.14 Ma) (Fig. 9, Table 4)

Most grains are subrounded in shape (17LM14-1.1) and a few are elongated in shape (17LM14-12.1). Fractures across the grains and embayments along rim/core and grain boundaries are common. There are some areas of dark CL that may or may not be inclusions. Only rim and core domains are found in 17LM14 zircons. 17LM14 rims are rounded to subhedral, thin, dark, and homogenous in CL (17LM14-17.1). 17LM14 cores are rounded to subhedral and have bright to dark CL with chaotic and/or homogenous textures (17LM14-13.1). Faded OZP is only found in the three excluded discordant grains of the 17LM14.

Twenty zircon grains were analyzed from sample 17LM14 with 22 analyses. All U/Pb ages for 17LM14 are taken from the core domains of the zircons. Dates for concordant or near-concordant zircon cores from sample 17LM14 range from 1110.3 ± 8.9 to 942.3 ± 6.3 Ma with a weighted mean age of 1045.2 ± 0.14 Ma (Table 3; Fig. 9d). Three grains 17LM14-6.1, -9.1 and -10.1 are excluded from age estimates because they have relatively high Fe and are discordant (Fig. 9d). Zircons gave Th/U ratios of 0.00724 to 0.06440 for all cores. See the Zircon Trace Element section below for 17LM14's REE and trace element analysis (Fig. 7A-d and 8). Zircons displaying chaotic domains have a weighted mean age of 1049.07 ± 0.16 Ma. Zircons with homogeneous domains have a weighted mean age of 1029.39 ± 0.33 Ma.

Trace Element Geochemistry

All zircons from the four samples have a positive sloping trend increasing from light rare-earth elements (LREE) to heavy rare-earth elements (HREE). Most zircons have a positive Ce anomaly, a weakly negative Eu anomaly, and an enrichment of HREE relative to the LREE (Fig. 7A; Table 3). Zircon trace element plots show a significant amount of variability in the LREE on the orders of 2+ magnitude (Fig. 7A) and two populations of HREE slopes in AD01 and 17LM01.

Titanium-in-Zircon Thermometry

Titanium-in-zircon thermometry is used to link temperature to time in metamorphic rocks (Chen and Zheng, 2017) and results in retrograde path temperatures. Ti-in-zircon temperature estimates for metamorphic zircon crystallization fall between 608 and 683 °C (Fig. 8b) with three exceptions, 17LM07-12.1 at 855 °C, AD01-16.1 at 582 °C, and 17LM14-6.1 at 664 °C. Metzger et al. (2022) Ti-in-zircon estimates from metamorphic and anatectic zircons fall between 734 and 790 °C and magmatic zircons fall between 809 and 981 °C. My zircon temperatures are lower than Metzger's which suggests that my zircons are recrystallized after the UHT conditions.

DISCUSSION

Zircon Interpretations

Zircon textures can be interpreted and classified into “magmatic” or “metamorphic” based on the CL brightness, the CL textures, the character of the domain where the analysis came from, the presence of faded OZP, the grain habit and the domain habit. “Magmatic” zircon domains have well-developed growth zoning as either OZP and/or sector zoning resulting from trace element variations as the zircon crystallizes from a magma, and most form subhedral to euhedral crystals (Corfu et al., 2003; Hoskin and Schaltegger, 2003). “Metamorphic” zircons have a variety of CL textures influenced by their crystallization from solid-state metamorphism, growth from a fluid, or recrystallization of an igneous core and are often subrounded (Corfu et al., 2003; Hoskin and Schaltegger, 2003). Growth of zircon in the presence of melt would also explain the general lack of distinctive round anhedral zircon morphologies usually found in metamorphic rocks which formed below melting temperatures (Corfu et al., 2003). My LM zircon domains have rounded to subhedral shapes with a variety of CL. Inherited zircon cores vary in CL from other rim, mantle or core domains and are distinctly overprinted by younger domains. Only one inherited core was identified in my samples.

<u>Evidence for Anatexis</u>

Rims represent the final stage of recrystallization (Pidgeon et al., 1998) and suggest the presence of a melt and crystallization from the melt. Zircon rim domains of thin, dark, homogenous CL are evidence of crystallization from an anatectic melt. No U-Pb ages were taken from my rims and therefore we have not directly dated the recrystallization event that formed them but we can infer that these were formed during a final stage of metamorphism after the core events. Metzger et al. (2022) analyzed dark homogenous rims that are similar to mine but are thicker which allowed for U-Pb SHRIMP analysis. Rim domains from pegmatitic leucosomes range from 1019 ± 12 to 959 ± 14 Ma, with one outlier (1085 ± 13 Ma) are the youngest dates and suggest that this pegmatitic leucosome formed during cooling and crystallization from an anatectic melt on the retrograde P-T path and represents the most recent metamorphism at Ledge Mountain (Reeder, 2017; Metzger et al., 2022). My pegmatitic leucosome (17LM01) ages are older (WMA of 1036 ± 0.2 Ma) but come from core domains. Pegmatitic leucosome zircons with chaotic domains have a weighted mean age of 1045.5 ± 0.27 Ma and with homogenous domains have a weighted mean age of 1032.16 ± 0.2 Ma.

Embayments along cores are evidence of dissolution and support the presence of anatectic melt and rims as recrystallization of the anatexis. Petrographic textural evidence also signifies crystallization in the presence of former melt is common throughout migmatite samples seen in the peritectic garnets with lobate quartz inclusions, Fe-Ti oxide, biotite, muscovite, and feldspar inclusions; the melt films around grain boundaries; and presence of muscovite.

Evidence of Metamorphic Recrystallization and/or Anatexis

Oscillatory zoning is a primary magmatic zircon growth event and the fading or disruption of the OZP is a secondary event indicating solid-state recrystallization during metamorphism (Pidgeon et al., 1998; Hoskin and Black, 2000; Corfu et al., 2003; Hoskin and Schaltegger, 2003). Faded OZP is a common feature in LM zircon core domains; found in all 17LM01 zircons, most 17LM07 zircons, some AD01 and 17LM14 zircons, and most of Metzger et al. (2022) zircons. Metamorphic (or anatectic) zircons have weak zoning compared to magmatic zircons with OZP and sector zoning (Rubatto, 2017). Hoskin and Black (2000) and Pidgeon et al. (1998) suggest that recrystallization of the homogeneous rims and fading of OZP are related.

Zircon cathodoluminescence patterns known as “fir tree” and “soccer ball” grain shapes were identified in migmatitic metapelites in the eastern Highlands by Bickford et al. (2008). These textures were not found in my or Metzger’s zircons. Evidence for hydrothermal growth in zircons focusing on high-U alteration overgrowth onto low-U zircon that are often found as high-U embayments in zircon cores suggest these overgrowths formed from aqueous fluids by recrystallization, metasomatism, or dissolution and reprecipitation at low pressures and temperatures (Corfu et al., 2003). These hydrothermally precipitated textures are not found in my or Metzger’s zircons. Additionally, faded OZP is not consistent with fluid dissolution, external fluid or melt (Hoskin and Black, 2000).

Evidence for and Variability of Metamorphism in Zircon

Zircon core domains include homogeneous and chaotic zoning. A wide variety and complexity of textures is common for zircon in high-grade metamorphic rocks and can be a result of variation in physico-chemical conditions, the duration of each metamorphic event, and are caused by modifications of pre-existing structures and/or by growth of new zircon (Corfu et al., 2003). Granulite-facies zircons tend to be characterized by very chaotic textures but it is also not uncommon to find zircons or domains of zircons that are completely or nearly homogeneous (Corfu et al., 2003). The most extreme textural types have abstract and chaotic designs that combine stepwise growth patterns with flow structures.

Homogeneous domains are common in LM zircons. Zircon formed in sub-solidus conditions show homogenous or “cloudy” and “irregular” zonation (Rubatto, 2017). Low-luminescent zircon domains are the result of metamorphic transformation rather than new zircon growth which is supported by the lack of igneous growth textures, dark featureless zones (Siebel et al., 2012). Granulite metamorphism erases initial (magmatic) zircon patterns (Siebel et al., 2012). In the case of domains that are homogeneously dark in CL, they can be suspected to be free of zoning because the luminescence may be poisoned by high trace-element contents or by metamictization (Siebel et al., 2012). Homogeneous domains tend to have lower U concentrations than chaotic domains. Small areas of homogeneity are also found within domains, this suggests local recrystallization (Corfu et al., 2003). I have interpreted these homogenous domains as a result of subsolidus (solid state) metamorphic recrystallization.

Chaotic zoning is a notable feature in my zircons and seen as “complex” domains in Metzger et “mosaic” textures that indicated metasomatic replacement of low-U domains by zircon richer in U in late to post magmatic recrystallization of zircons. Hoskin and Black (2000) identified “spongy” domains ial. (2022). Chaotic zoning is common in granulite facies zircons (Corfu et al., 2003). Chaotic is defined by many different words: mosaic, spongy, disturbed. Corfu et al. (2003) identified n zircons in Hacker et al. (1998). These zircons also feature the high-U overgrowths on low-U core domains. Hoskin and Black (2000) interprets these “spongy” domains as unequivocally aqueous fluid induced recrystallization. As previously stated, we do not have high-U overgrowths in our zircons but this could possibly suggest aqueous metamorphism. Rubatto et al. (2012) observed “peculiar mosaic” zoning which they attribute to metamict or recrystallized zircons. Rubatto (2017) cited a chaotically zoned zircon with “disturbance of the original zoning” from a micashist in the Sulu orogeny, China, (from Zhang et al. 2009) that was interpreted as metamorphic fluid alteration.

Pidgeon et al. (1998) features zircons with “curved” zoning and illustrated a sequence of igneous OZP formation and then metamorphic disruptions to OZP followed by transgressive recrystallization fronts. Pidgeon et al. (1998) suggests two interpretations for these “curved” zones. Similar “curved” textures have been identified in plagioclase have been interpreted as flow domain structures (Bryan and Pearce, 1994; cit. in Pidgeon et al., 1998) or a secondary remobilization and concentration of trace elements from a late stage interaction between zircon and fluids to develop these “curved” textures (Pidgeon et al., 1998).

Rubatto et al. (2008) defined a textural transformation of magmatic crystals into “mosaic-like, irregular” zoning initiated along fractures and grain boundaries “consuming” the crystals and occasionally preceding the formation of zircon microcrystals. Rubatto et al. (2008) interprets this progressive transformation as associated with a volume revolution that is accommodated by dissolution of zircon into a fluid/melt phase and transport outside the system. This dissolution-reprecipitation process occurred within the zircon contrary to other dissolution and reprecipitation process that produce overgrowths on zircon cores like what is seen in high-grade rocks where melt is present (Corfu et al., 2003; Rubatto et al., 2008).

The best interpretations for the mechanisms creating chaotic zoning are fluid induced alteration or recrystallization (Hoskin and Black, 2000; Rubatto, 2017), recrystallization driven by dissolution-reprecipitation (Rubatto et al. 2008), or migration and precipitation as a late stage interaction between zircon and fluids (Pidgeon et al., 1998). I have interpreted these chaotic textures as a result of recrystallization in the presence of an anatectic melt.

The zircon CL textures are classified as chaotic and homogeneous to look for patterns that might explain zircon crystallization history. I analyzed the zircon chemistry, REE patterns and Ti-in-zircon temperature along with U-Pb geochronology.

<u>Zircon Age Distributions</u>

Most of the concordant zircon dates collected from core domains range from 1110.3 ± 8.9 to 930.2 ± 34.1 Ma. The weighted mean age of all my concordant or near concordant zircon cores range from 1045.68 ± 0.13 to 1036.9 ± 0.2 Ma which places this event within the mid-

Ottawan. This is a very small range of time however we see a great variation in CL brightness and zoning patterns. Dividing these dates into the two metamorphic textures – chaotic and homogenous – we see two age populations for the two metamorphic stages for LM migmatites.

Dates for concordant or near-concordant zircon cores from sample AD01, an interlayered melanosome and leucosome, range from 1118.21 ± 21.13 to 930.2 ± 7.5 Ma with a weighted mean age of 1045.68 ± 0.13 Ma. Two older grains have a weighted mean age of 1082.87 Ma ± 0.65%. Chaotic core domains range from 1118.21 ± 21.13 to 989.55 ± 17.81 Ma with a weighted mean age of 1056.4 ± 0.2 Ma. Homogeneous domains in AD01 range from 1054.38 ± 11.44 to 930.18 ± 5.52 Ma with a weighted mean age of 1023.16 ± 0.22 Ma.

Dates for concordant or near-concordant zircon cores from sample 17LM01, a pegmatitic leucosome, range from 1074.1 ± 6.9 to 930.2 ± 34.1 Ma with a weighted mean age of 1036.9 ± 0.2 Ma. Chaotic core domains in 17LM01 range from 1074.09 ± 6.89 to 930.18 ± 34.15 Ma with a weighted mean age of 1045.5 ± 0.27 Ma. Homogeneous domains in 17LM01 range from 1051.98 ± 13.25 to 944.41 ± 16.55 Ma with a weighted mean age of 1032.16 ± 0.2 Ma.

Dates for concordant or near-concordant zircon cores from sample 17LM07, an interlayered melanosome and leucosome, range from 1049.7 ± 14.5 to 994.7 ± 6.2 Ma with a weighted mean age of 1037.6 ± 0.2 Ma; all are homogeneous domains.

Dates for concordant or near-concordant zircon cores from sample 17LM14, an interlayered melanosome and leucosome, range from 1110.3 ± 8.9 to 942.3 ± 6.3 Ma with a weighted mean age of 1045.2 ± 0.14 Ma. Chaotic core domains in 17LM14 range from 1110.33 ± 8.86 to 942.34 ± 6.27 Ma with a weighted mean age of 1049.44 ± 0.16 Ma. Homogeneous domains in 17LM14 range from 1029.99 ± 10.48 to 966.15 ± 23.41 Ma with a weighted mean age of 1022.86 ± 0.37% Ma.

Chaotic domains range from 1056.4 ± 0.2 to 1045.5 ± 0.3 Ma (weighted mean ages) and are a result of recrystallization from fluid driven metamorphism during anatexis. The homogeneous domains are a result of granulite-facies recrystallization from an anatectic melt from 1037.78 ± 0.17 to 1022.86 ± 0.33 Ma (weighted mean ages). Chaotic domains tend to be older than homogeneous domains. The best example of homogenous and chaotic age differences is seen on Fig. 9d where all 17LM14 chaotic domains are older than homogeneous domains. The combinations of difference in U-Pb ages and variation of CL textures can be used to interpret as two different recrystallization events.

Trace Element Analysis of Zircon

Thorium/Uranium (Th/U) ratios are one of the few consistent measurements for distinguishing igneous and metamorphic zircons. All LM zircons have Th/U ratios below 0.07 (Fig. 8a., Table 3). Th/U ratio <1.0 suggests metamorphic zircons (Hoskin and Schaltegger, 2003, Peck et al., 2018). Yttrium/gadolinium (Yb/Gd) ratios range from 0.94 - 157 and express heavy rare earth element abundance. Garnet preferentially incorporates heavy rare earth elements, so Yb/Gd ratios >40 result from growth without garnet. The majority 17LM14 grains plot close to or above the Yb/Gd = 40 line, signifying their growth without garnet which is further supported by the lack of garnet in the thin section. Depletion of Yb means zircon is grown in equilibrium with garnet (Grimes et al., 2015); seen in all AD01, most 17LM01, and most 17LM07 zircons on Fig. 8a. This is further confirmed by garnet found in AD01 and 17LM07 thin sections. Metzger et al. (2022) metamorphic and complex zircons all plot about the Yb/Gd >40 line, like 17LM14, which is interpreted as garnet in a stable statement during zircon recrystallization.

The U/Ce versus Th plot in Figure 8c shows concentrations for chaotic core domains (X) and homogenous domains (circle), all zircons fall in the metamorphic or anatectic field (Hoskin and Schaltegger 2003). Homogenous zircons have a lower average Th concentration than chaotic zircons. There is a slight trend with age and Ti-in-zircon temperatures among chaotic and homogenous zircons; chaotic line older and hotter and homogenous lean younger and cooler (Fig. 8b). Zircon textures suggest that recrystallization from an anatectic melt happened later and further along the retrograde path than fluid driven dissolution-reprecipitation chaos.

Most of my zircons have a weakly negative Eu anomaly (~0.3 to 2) with the exception of a few AD01 grains that also have higher REE concentrations and three 17LM07 zircons have positive Eu anomalies that also have higher LREE and lower HREE concentrations. Weak Eu anomalies are typical of granitic rocks, HT metamorphic rocks, and granulite facies zircons when they are grown in equilibrium with garnet (Hoskin and Black, 2000; Rubatto, 2002; 2017, Rubatto et al., 2008; 2012; and Wu, 2020). A positive Ce anomaly cannot be calculated due to the lack of Pr concentration data and therefore we should not put too much emphasis on Ce anomalies but Ce will be analyzed relative to La and Nd. The majority of zircons have the typical positive Ce anomaly. The positive Ce-anomaly and negative Eu-anomaly is partly controlled by oxygen fugacity. The Eu-anomaly is also connected to plagioclase fractionation which depletes Eu from the magma prior to and/or during zircon crystallization (Hoskin and Schalteger, 2003) or its coexistence with K-feldspar (Rubatto, 2002).

Trace Element Patterns

The light REE (LREE) slope is defined by Samarium/Lanthanum (Sm/La_N) ratio, greater values representing a steeper slope (Hoskin and Schaltegger, 2003). There is a lot of variation in concentration on the orders of magnitude in the LREEs in my samples (~1 to 599). AD01 zircons spread over three orders of magnitude; Sm/La_N values range from ~0.6 to 593 with one exceptionally steep slope for AD01-3.1 (Sm/La_N=3748). Higher concentration LREE grains tend to be younger (1051.7 ± 8.9 to 930.2 ± 7.5 Ma), have positive Eu anomalies, and are more elongated grains. 17LM01 LREE trace element concentrations spread over two orders of magnitude; Sm/La_N values range from ~2 - 459. Lower LREE values are associated with older grains, the opposite is true for AD01 zircons. Higher LREE values are associated with negative Ce anomalies. 17LM07 zircons have little variability in the pattern of LREE concentrations; Sm/La_N values range from ~6 - 275 with one exceptionally steep 17LM07-15.1 (599). 17LM14 zircons spread over two orders of magnitude; Sm/La_N values range from ~0.1 - 24. There is a lot of variability in the LREE concentrations. Zircons with higher LREE concentrations tend to have negative Ce anomalies relative to La and Nd and tend to be more elongated grains. The variability in the LREE on the orders of 2+ magnitudes can be explained by different degrees of recrystallization and possible retention of the protolith chemistry during recrystallization. Light rare-earth elements are more readily expelled during recrystallization and therefore a presence of both enriched LREE in recrystallized zircons is likely a result of “memory” of the igneous zircon (Hoskin and Black, 2000). This scattering of LREE concentrations from different degrees of recrystallization in our grains is compared to Hoskin and Black (2000) in Fig. 7B-c.

The HREE slope is defined by the Lutetium/Gadolinium (Lu/Gd_N) ratio, greater values representing a steeper slope (Hoskin and Schaltegger, 2003). I don’t have Lu concentrations so I have defined HREE slopes by Yb/Gd_N. AD01 zircons Yb/Gd_N values range from ~1 - 44. There are two populations in the HREE; those with steep slopes (average Yb/Gd ratio = 18.7) and those with flat slopes (average Yb/Gd ratio = 2.9; Fig. 7A-a). 17LM01 zircons Yb/Gd_N values range from ~0.9 - 32, with one exceptionally steep zircon 17LM01-17.1 (141) which has a concave slope, a negative Ce anomaly, and a weakly positive Eu anomaly unlike all the others. There are two populations in the HREE; those with steep slopes (average Yb/Gd = 21.58) and those with flat slopes (average Yb/Gd = 2.2). 17LM07 zircons Yb/Gd_N range from ~16 - 64 and 17LM14 zircons Yb/Gd_N range from ~15 - 157. There is little variability in the slopes and concentrations of HREE from 17LM07 and 17LM14. There doesn't seem to be a correlation with HREE and LREE concentrations; higher HREE concentrations don't always associate with high LREE concentrations.

Figure 7B shows all of the Ledge Mountain zircons plotted against other representative REE patterns for interpretation (Hoskin and Black, 2000; Hoskin and Schaltegger, 2003; Rubatto, 2017; Metzger et al., 2022). Overall, REE concentrations are lower for the four samples in this study compared to others. Comparison of my zircon REE patterns to igneous zircon patterns are modeled as "magmatic zircon" in Fig. 7B-a (Rubatto, 2017), as "igneous protolith" in Fig. 7B-c (Hoskin and Black, 2000), and as "prismatic crystal growth in equilibrium with melt" in Fig. 7B-d (Hoskin and Schaltegger, 2003). My zircons do not show as strong of Ce or Eu anomalies nor as high of HREE concentrations relative to LREE concentrations as the modeled igneous zircons which confirms my zircons are not igneous. The presence of an Eu anomaly and the lack of HREE depletion in some of my zircons suggests zircon grew with plagioclase, at retrograde P-T conditions (Rubatto, 2002).

AD01 and 17LM01 both have populations of flat slopes in the HREE, compared to "subsolidus growth in equilibrium with garnet" in Fig. 7B-d (Hoskin and Schaltegger, 2003) and "granulite zircon" in Fig. 7B-a (Rubatto, 2017) this depletion of HREE that lead to a flat or negative slope is a result of subsolidus growth of zircon and garnet (Hoskin and Black, 2000; Rubatto, 2002; Hoskin and Schaltegger, 2003). Zircons that grow in garnet-rich assemblages where HREE are sequestered in garnet, will show a relatively flat to negative HREE pattern compared to magmatic zircon patterns (Rubatto, 2002; 2017).

Rubatto (2008) saw a trend of “mosaic” zoning resembling chaotic zoning that showed a weakly negative Eu anomaly, a strong depletion in middle-REE (MREE) with respect to HREE, and being richer in Sr and poorer in L-MREE compared to magmatic zones. When comparing my chaotic zircons to magmatic zircons from Rubatto (2017) and prismatic zircons from Hoskin and Schaltegger (2003), I see the same pattern identified by Rubatto et al. (2008) with a weakly negative Eu anomaly, a depletion of MREE with respect to HREE and poorer in L-MREE than magmatic zircons (Fig. 7B-a and d).

The populations of flat HREE though similar in REE concentrations are not similar in CL texture. In CL, 17LM01 zircon cores are mostly elongate, with medium brightness, and a homogenous texture; all have faded OZP and chaotic zoning is rare. In CL, AD01 zircons cores are mostly rounded with a few elongate, bright to medium bright, homogenous and chaotic. Faded OZP is seen but not as common in AD01. Chaotic zoning is common in AD01. I was unable to find characteristics (chaotic vs homogenous domains, elongate vs rounded grains, younger vs older grains, etc.) that could explain their different REE slopes.

My zircon REE patterns are similar to Metzger et al. (2022); both follow similar slopes, with moderately sloped LREE and steeper HREE, Ce anomalies relative to La and Nd and weak Eu anomalies (Fig. 7B-b). However, the zircon trace element patterns in Metzger et al. (2022) have higher Ce concentrations (relative to La and Nd) and Metzger et al. (2022) does not have as much variability in LREE concentrations (on orders of magnitude). Most notably, Metzger et al. (2022) does not have the populations of flatter HREE zircons seen in AD01 and 17LM01. Using the interpretations that flat or negative slopes are a result of subsolidus growth of zircon and garnet (Hoskin and Black, 2000; Rubatto, 2002; Hoskin and Schaltegger, 2003).

There is a trend between inconstancy in REE patterns and chaotic textures. Zircons from sample 17LM07 have mostly homogenous core domains and have the least amount of variability in the slope and concentrations of REE. AD01, in contrast, has a lot of variability (spread across 3 orders of magnitude) in the LREE and HREE and also shows all types of CL textures, and mostly chaotic zoning. 17LM14 has a lot of inconsistency in LREE and shows a mix of CL textures. 17LM01 has a lot of inconsistency in LREE and some in the HREE and shows a mix of CL texture. Overall, this suggests that there is a correlation between variability in REE and variability in CL textures.

Timing of Metamorphism

Our U-Pb geochronology analysis of the migmatite samples (three interlayered melanosome and leucosome and one pegmatitic leucosome) from Ledge Mountain set metamorphic events during the mid- to late-Ottawan phase of the Grenvillian Orogeny in the central Adirondack Highlands.

New U-Pb zircon SHRIMP data of pegmatitic leucosome zircons range from 1074.09 ± 6.9 to 930.2 ± 34.1 Ma with a weighted mean age of 1036.9 ± 0.2 Ma. Chaotic domains in 17LM01 range from 1074.09 ± 6.89 to 930.18 ± 34.15 Ma with a weighted mean age of 1045.5 ± 0.27 Ma. Homogeneous domains in 17LM01 range from 1051.98 ± 13.25 to 944.41 ± 16.55 Ma with a weighted mean age of 1032.16 ± 0.2 Ma. Metzger et al., 2022 suggest that pegmatitic leucosomes formed as the most recent crystallization of anatectic melt at LEdge Mountain. This is reflected by the young pegmatitic leucosome rim ages found in metzger et al. (2022; 1019 ± 12 to 959 ± 14 Ma). Pegmatitic leucosomes may have recorded three metamorphic events; first recrystallization in the presence of anatectic melt during exhumation affecting resulting in chaotic core domains around 1046 Ma, followed by a solid-state recrystallization resulting in a homogeneous core domain around 1032 Ma, and lastly a melting event affecting rims around 1019 to 959 Ma.

New U-Pb zircon SHRIMP data place metamorphism from interlayered melanosome and leucosome zircons from 1110.2 ± 21.1 to 930.2 ± 34.1 Ma with a weighted mean age of 1045.68 ± 0.13 to 1037.6 ± 0.2 Ma (Fig. 9; Table 4). Analyses of zircons displaying chaotic domains give a mean age of 1056.0 ± 0.2 to 1045.5 ± 0.3 Ma which possibly records recrystallization driven by presence of an anatectic melt or by localized dissolution-reprecipitation (Pidgeon et al., 1988; Rubatto et al., 2008; 2017). Analyses from homogeneous domains give a mean age of 1037.78 ± 0.17 to 1022.86 ± 0.33 Ma which represents recrystallization after anatexis. These U-Pb ages date the granulite facies metamorphism during (1056 to 1046 Ma) and after (1038 to 1023 Ma) anatexis.

Mechanism of Metamorphism

There is evidence to support that different mechanisms resulted in the chaotic and the homogeneous domains. The variability in LREE on the scale of two or more orders of magnitude suggests different degrees of recrystallization occurred (Hoskin and Black, 2000). The two populations of HREE slopes (the enriched and the depleted), one suggesting crystallization in subsolidus conditions with garnet (HREE depletion) and the other suggesting zircon growth at retrograde P-T conditions with plagioclase present (HREE enrichment; Hoskin and Black, 2000; Rubatto, 2002; 2017; Hoskin and Schaltegger, 2003) also suggest different forms of metamorphism.

Chaotic zoning occurs as variable CL brightness and textures. The metamorphic mechanisms for chaotic textures are not well explained and further understanding of the process may lead to more definitive answers. Possible explanations involve fluid-induced alteration creating flow-like textures (Pidgeon et al., 1998), fluid induced recrystallization (Hoskin and Black, 2000), or a secondary remobilization and concentration of trace elements from a late-stage interaction with fluids (Pidgeon et al., 1998). Another explanation involves recrystallization driven by a dissolution-reprecipitation process within the zircon (Rubatto et al., 2008) which is further supported by evidence of a fluid/melt phase when comparing the loss of LREE- to MREE compared to magmatic zircons. Metzger et al. (2022) pseudosection models showed a presence of at least ~15-30% melt during buoyancy-driven exhumation and decompression which supports the theory of melt contributing to the chaotic textures. We don't see evidence of external fluid but we do see evidence of anatectic melt. Therefore, we have interpreted chaotic domains as a result of recrystallization in the presence of the anatectic melt during exhumation.

Pidgeon et al. (1998) also interpret a sequence of zircon growth and recrystallization explaining the disruption of OZP that lead to chaotic textures. The next step in this process could involve more recrystallization of chaotic textures leading to homogenous textures. The younger ages of homogeneous domains (1037.78 ± 0.17 to 1022.86 ± 0.33 Ma; Fig. 9A-D, Table 4) supports this idea that further recrystallization has erased the chaotic textures. The younger ages from the homogenous domains could also suggest that these domains experienced longer periods of metamorphism than the chaotic domains. As if in stages, first igneous OZP grows within the zircon, then a presence of fluid results in dissolution and reprecipitation that creates chaotic zoning, and then with further external forces such as increased temperatures or prolonged exhumation domains become homogenous.

Comparison with Zircons from Other UHT Complexes

Ledge Mountain metamorphism took place in the mid-Ottawan phase of the Grenvillian orogeny. U-Pb ages represented by chaotic zircon domains place anatexis and exhumation from 1057.0 ± 0.2 to 1045.2 ± 0.14 Ma. U-Pb ages represented by homogenous core domains place post-anatexis and recrystallization from 1037.78 ± 0.17 to 1029.39 ± 0.33 Ma. These dates coincide with previously recorded estimates of other areas of UHT metamorphisms in the central Highlands including Gore Mountain, Snowy Mountain, and Oregon dome. Gore Mountain garnet amphibolites experienced UHT conditions (9-10 kbar, 950 ± 40℃) at 1053.9 ± 5.4 Ma (Shinevar et al., 2021). Granulite facies metamorphism was recorded at Oregon dome at 1048 ± 10 Ma and at Snowy Mountain at 1031 ± 30 Ma (Hamilton et al., 2004). This also coincides with other metamorphism in the Highlands including recorded in zircons from anorthosite in the Marcy Massif at 1050-1035 Ma (Peck et al., 2018), metamorphic zircon rims from Hawkeye Granite Gneiss and Lyon Mountain Granite Gneiss dated from 1080-990 Ma (Aleinikoff et al., 2021).

CONCLUSION

New U-Pb zircon SHRIMP geochronology and zircon textural data confirm mid- to late Ottawan metamorphism and anatexis in the central Highlands. Ledge Mountain is characterized by UHT migmatites that underwent peak PT conditions (960-1025°C and 11-12.5 kbar) and a presence of at least 15-30% melt during exhumation and decompression (Metzger et al., 2022). My samples include three interlayered melanosome and leucosomes and one pegmatitic leucosome. Zircons are rounded to subhedral with two domains, an outer rim and an inner core. Granulite facies zircons texturally are known to range from homogeneous to chaotic.

Homogeneous domains are nearly one consistent brightness, usually medium bright in CL and are rounded to subhedral. These homogeneous domains are a result of solid-state metamorphic recrystallization following UHT events from 1036.5 ± 0.2 to 1022.9 ± 0.4 (WMA). My conclusions are supported by Metzger et al. (2022) that showed solid-state metamorphism recrystallization following anatexis from 1045 to 1036 Ma.

Chaotic textures in Ledge Mountain have not been previously identified and little is understood about the process of their formation. Chaotic domains range in CL from bright to dark and follow no patterns and are rounded to subhedral. These chaotic domains are a result of fluid-driven recrystallization during anatexis from 1057.0 ± 0.2 to 1045.5 ± 0.3 Ma at date the timing of anatexis during exhumation of the gneiss dome of the central Highlands. These new older chaotic domain age populations were not seen in Metzger et al. (2022) and broaden the timeline of the anatectic and metamorphic process at Ledge Mountain. Chaotic zircon CL textures are common features of granulite-facies metamorphism (Corfu et al., 2003). Similar chaotic zircon textures are found in other UHT settings including in high-grade metagranitoids from Queensland, Australia (Hoskin and Black, 2000); granulite-facies in the Reynolds Range, central Australia (Rubatto et al., 2001; 2002); in eclogite-facies rocks of the Lanzo massif, northwestern Italy (Rubatto et al., 2008); and metamorphic rocks of Sikkim, Eastern Himalaya (Rubatto, 2012).

TABLES

TABLE 1. DESCRIPTIONS OF FOUR REPRESENTATIVE LEDGE MOUNTAIN SAMPLES USED			
Sample number	Coordinates (latitude/longitude)	Rock Name	Mineral Assemblage
AD01	43°48'38"N, 74°18'32"W	Interlayered Melanosome and Leucosome	Qz + Pl + Ksp + Bt + Grt + Sil + Ms + Trace (Rt + Ilm + Zrn + Mag ± Hc ± Ap ± Mnz)
17LM01	43°48'39"N, 74°18'45"W	Pegmatitic Leucosome	Qz + Pl + Bt + Ksp/Mc + Ms + Opq (Ilm + Mag) + Zrn + Chl + Rt + Sil
17LM07	43°48'38.1"N, 74°18'31.9"W	Interlayered Melanosome and Leucosome	Qz + Ksp + Pl + Mc + Sil + Grt + Bt + Opq (Ilm + Mag) + Myrmekite + OPX + Ser + Zrn + Ms + Chl + Hc
17LM14	43°48'35.2"N, 74°18'19.8"W	Interlayered Melanosome and Leucosome	Pl + Ksp/Mc + Qz + Bt + Opq (Ilm + Mag) + Myrmekite + Zrn + Ms + Chl + Sil

Note: Mineral abbreviations after Whitney and Evans (2010): Alm-almandine; Ap-apatite; Bt-biotite; Grs-grossular; Grt-garnet: Hc-hercynite; Ilm-ilmenite; Ksp-K-feldspar; Mag-magnetite, Mnz-monazite; Ms-muscovite; Pl-plagioclase; Prp-pyrope; Qz-quartz; Rt-rutile; Sil-sillimanite; Sps-spessartine; Zrn-zircon.

Table 1. Descriptions of four representative Ledge Mountain samples used

TABLE 2. WHOLE-ROCK X-RAY FLUORESCENCE AND INDUCTIVELY COUPLED PLASMA MASS SPECTROMETRY MAJOR AND TRACE ELEMENT ANALYSES FOR REPRESENTATIVE LEDGE MOUNTAIN MIGMATITES

Sample number	AD01a	AD01b	AD01b replicate	17LM01	17LM07	17LM14
Unnormalized major elements (wt%)						
SiO2	71.71	71.72	71.74	71.40	71.55	69.48
TiO2	0.59	0.65	0.65	0.50	0.65	0.66
Al2O3	14.08	14.57	14.59	14.57	13.26	13.14
FeO*	4.53	4.77	4.77	3.89	5.20	5.34
MnO	0.08	0.07	0.07	0.06	0.22	0.05
MgO	0.50	0.48	0.51	0.31	0.27	0.46
CaO	1.94	1.80	1.81	2.78	0.27	2.39
Na2O	1.78	1.56	1.57	3.69	0.88	1.93
K2O	3.59	2.88	2.88	1.42	6.47	4.78
P2O5	0.11	0.12	0.12	0.10	0.13	0.15
Total	98.90	98.61	98.70	98.73	98.89	98.39
LOI%	0.63	0.66	0.66	0.72	0.63	1.06
Unnormalized trace elements (ppm)						
Ni	0.00	0.00	0.00	4.00	5.00	3.00
Cr	2.00	2.00	1.00	2.00	1.00	7.00
Sc	8.00	7.00	7.00	5.00	15.00	9.00
V	6.00	8.00	7.00	4.00	6.00	19.00
Ba	660.00	536.00	535.00	276.00	945.00	903.00
Rb	138.00	115.00	115.00	34.00	196.00	164.00
Sr	124.00	106.00	106.00	170.00	115.00	146.00
Zr	789.00	820.00	820.00	772.00	920.00	538.00
Y	83.00	79.00	79.00	104.00	207.00	62.00
Nb	28.10	29.00	29.10	26.20	42.40	17.40
Ga	25.00	28.00	30.00	24.00	18.00	24.00
Cu	0.00	0.00	0.00	2.00	0.00	2.00
Zn	180.00	207.00	206.00	10.00	48.00	68.00
Pb	21.00	17.00	16.00	7.00	14.00	15.00
La	84.00	93.00	92.00	76.00	66.00	61.00
Ce	177.00	201.00	204.00	160.00	144.00	129.00
Th	15.00	19.00	19.00	15.00	14.00	16.00
Nd	87.00	106.00	104.00	78.00	72.00	65.00
U	5.00	6.00	5.00	4.00	4.00	4.00
sum tr.	2433.00	2380.00	2374.00	1774.00	2832.00	2252.00
in %	0.24	0.24	0.24	0.18	0.28	0.23
sum m+t	99.15	98.85	98.94	98.91	98.41	98.62
M+Tr oxides	99.20	98.91	99.00	98.95	99.24	98.66
w/LOI	99.83	99.57	99.66	99.68	99.87	99.73
if Fe3+	100.33	100.10	100.19	100.11	100.45	100.32

Note: M – Major elements; M + Tr – major and trace oxides; Tr – trace elements; LOI – loss on ignition. Sample AD01a is referred to in some places in the text and figures as AD01.
*Total Fe

Table 2. Whole-rock X-ray fluorescence and inductively coupled plasma mass spectrometry major and trace element analyses for representative Ledge Mountain migmatites

TABLE 3. ZIRCON TRACE ELEMENT ANALYSES FOR REPRESENTATIVE LEDGE MOUNTAIN MIGMATITES

Analysis Spot Number	La (ppm)	Ce (ppm)	Nd (ppm)	Sm (ppm)	Eu (ppm)	Gd (ppm)	Dy (ppm)	Er (ppm)	Yb (ppm)
McDonough & Sun (1995)	237	613	457	148	56.3	199	246	160	161
AD01-1.1	0.034	0.151	0.063	0.414	2.625	3.933	18.164	34.679	66.512
AD01-2.1	1.280	0.532	0.273	0.706	3.596	13.542	38.271	34.110	32.264
AD01-3.1	0.000	0.102	0.023	0.524	0.502	5.679	16.577	17.053	17.718
AD01-4.1	0.001	0.090	0.006	0.204	0.308	3.094	20.090	45.307	70.379
AD01-5.1	0.029	0.100	0.031	0.318	0.862	3.679	12.450	15.101	12.201
AD01-6.1	0.036	0.148	0.118	0.678	1.959	5.478	16.630	19.534	23.549
AD01-7.1	0.001	0.094	0.014	0.414	0.580	4.768	12.144	7.125	5.567
AD01-8.1	0.003	0.112	0.017	0.389	0.671	4.900	18.558	10.153	5.223
AD01-9.1	0.002	0.059	0.007	0.128	0.229	1.706	11.406	32.493	60.251
AD01-10.1	0.048	0.138	0.068	0.298	1.043	3.185	18.793	36.695	40.692
AD01-11.1	0.096	0.196	0.136	0.130	1.610	4.202	18.438	22.621	17.131
AD01-12.1	0.134	0.228	0.170	0.742	2.579	6.711	19.135	17.599	16.655
AD01-13.1	0.043	0.095	0.044	0.203	0.942	2.492	18.605	46.983	75.104
AD01-14.1	0.009	0.099	0.020	0.228	0.563	2.920	19.690	32.578	29.656
AD01-15.1	0.001	0.072	0.004	0.163	0.305	2.357	15.962	29.845	39.297
AD01-16.1	0.033	0.131	0.038	0.211	0.890	3.728	27.595	57.817	90.019
AD01-17.1	0.114	0.221	0.119	0.241	4.170	2.641	17.556	36.893	31.354
AD01-18.1	0.005	0.101	0.013	0.312	0.562	4.957	18.004	13.228	8.820
AD01-19.1	0.009	0.103	0.013	0.056	0.429	2.861	18.916	20.827	12.927
AD01-20.1	0.001	0.062	0.003	0.065	0.228	1.523	13.600	38.552	67.896
AD01-21.1	0.004	0.102	0.011	0.274	0.447	4.743	26.688	46.685	69.793
AD01-22.1	0.010	0.104	0.017	0.260	0.511	3.367	17.794	17.876	12.850
AD01-23.1	0.001	0.112	0.019	0.478	0.651	5.747	16.942	12.956	13.019
AD01-24.1	0.124	0.242	0.087	0.318	2.703	4.520	19.371	19.061	14.861
AD01-25.1	0.000	0.006	0.002	0.004	0.467	1.194	21.391	36.001	47.504
AD01-26.1	0.185	0.305	0.406	1.300	7.312	5.613	21.944	38.998	51.148
AD01-27.1	0.007	0.104	0.011	0.173	0.565	3.221	21.029	29.112	27.127

AD01-28.1	0.063	0.153	0.080	0.523	1.709	4.001	23.693	39.801	56.180
AD01-29.1	0.077	0.178	0.130	0.464	1.988	4.489	18.067	18.200	18.469
17LM07-1.1	0.024	0.105	0.028	0.274	0.532	3.145	18.947	40.678	62.469
17LM07-2.1	0.001	0.102	0.011	0.277	0.295	3.811	27.394	71.473	124.622
17LM07-3.1	0.007	0.121	0.020	0.321	0.455	4.371	26.091	57.967	88.756
17LM07-4.1	0.011	0.094	0.019	0.237	0.512	2.752	15.831	31.354	44.875
17LM07-5.1	0.005	0.114	0.020	0.277	0.350	3.805	24.524	60.691	85.166
17LM07-6.1	0.001	0.088	0.006	0.224	0.275	3.137	21.167	46.622	70.448
17LM07-7.1	0.016	0.115	0.029	0.286	0.725	3.505	23.075	54.085	86.602
17LM07-8.1	0.064	0.172	0.163	0.609	1.845	3.691	23.590	56.087	89.943
17LM07-9.1	0.002	0.107	0.013	0.269	0.305	4.175	26.381	66.300	110.577
17LM07-10.1	0.021	0.109	0.037	0.321	0.630	3.812	24.295	58.833	92.021
17LM07-11.1	0.001	0.097	0.010	0.262	0.282	3.541	29.954	94.178	184.048
17LM07-12.1	0.103	0.207	0.220	0.804	2.442	4.317	23.580	51.742	80.805
17LM07-13.1	0.001	0.094	0.014	0.254	0.291	3.543	27.408	93.009	209.905
17LM07-14.1	0.028	0.070	0.067	0.173	0.812	2.166	18.258	40.153	60.691
17LM07-15.1	0.001	0.106	0.016	0.311	0.282	3.647	29.789	104.478	233.523
17LM07-16.1	0.002	0.085	0.007	0.149	0.296	3.280	19.090	37.779	56.026
17LM07-17.1	0.001	0.118	0.012	0.253	0.364	4.121	26.518	58.137	89.994
17LM07-18.1	0.006	0.101	0.033	0.257	0.609	2.994	20.251	47.571	77.651
17LM07-19.1	0.002	0.113	0.013	0.296	0.217	3.985	24.794	58.234	89.749
17LM07-20.1	0.002	0.094	0.012	0.185	0.297	3.968	23.756	56.929	91.976
17LM14-1.1	0.018	0.444	0.027	0.014	0.185	3.426	21.722	77.869	214.440
17LM14-2.1	0.075	0.445	0.069	0.208	0.437	4.018	25.411	93.514	266.523
17LM14-3.1	0.011	0.325	0.019	0.256	0.230	2.715	19.927	73.240	204.191
17LM14-4.1	0.515	0.553	0.391	1.275	0.859	5.093	23.974	80.395	211.946
17LM14-5.1	0.010	0.173	0.011	0.129	0.214	1.620	14.941	61.446	195.399
17LM14-6.1	2.131	0.526	0.346	0.121	0.727	1.656	14.498	60.248	197.641
17LM14-7.1	0.079	0.384	0.114	0.282	0.614	3.908	22.295	79.291	229.875
17LM14-8.1	0.283	0.182	0.164	0.076	0.366	2.516	18.482	79.128	249.476
17LM14-9.1	0.271	0.441	0.168	0.259	0.784	3.749	24.823	94.961	297.289
17LM14-10.1	0.102	0.437	0.018	0.105	0.370	4.395	32.254	121.776	362.597
17LM14-11.1	0.054	0.091	0.049	0.227	0.231	1.689	9.321	40.765	130.245

17LM14-12.1	0.453	0.257	0.298	0.913	0.822	3.603	14.391	48.108	148.722
17LM14-13.1	0.061	0.075	0.057	0.259	0.210	1.502	7.539	26.289	74.228
17LM14-14.1	0.012	0.067	0.014	0.124	0.163	1.034	6.742	25.564	70.016
17LM14-15.1	0.015	0.358	0.022	0.223	0.225	3.138	20.545	74.002	203.710
17LM14-16.1a	0.176	0.295	0.166	0.183	1.283	3.656	18.544	67.238	209.809
17LM14-16.1b	4.693	1.180	0.945	1.052	0.980	4.299	16.652	53.025	151.148
17LM14-17.1	0.004	0.063	0.006	0.057	0.086	0.757	7.780	34.544	112.738
17LM14-18.1	0.102	0.250	0.082	0.252	0.293	2.677	16.549	66.685	204.299
17LM14-19.1	0.638	0.341	0.489	1.804	1.165	5.083	11.609	27.837	77.674
17LM14-20.1	0.155	0.167	0.025	0.078	0.156	1.240	13.996	60.583	195.971
17LM14-21.1	0.128	0.207	0.132	0.439	0.493	2.397	16.594	64.607	207.102
17LM01-1.1	0.020	0.067	0.059	0.676	0.669	5.962	13.713	12.028	9.817
17LM01-1.2	0.001	0.050	0.020	0.487	0.420	5.935	14.146	12.072	10.313
17LM01-2.1	0.007	0.055	0.025	0.464	0.611	5.019	14.090	12.915	12.273
17LM01-3.1	0.002	0.061	0.018	0.410	0.404	4.755	29.278	72.956	127.445
17LM01-4.1	0.125	0.120	0.236	1.210	2.366	7.310	16.747	16.981	16.874
17LM01-5.1	0.002	0.039	0.011	0.290	0.247	3.262	13.070	17.491	20.254
17LM01-6.1	0.118	0.200	0.331	1.290	2.861	7.463	18.593	22.853	34.434
17lLM01-7.1	0.002	0.044	0.009	0.322	0.381	4.648	15.542	15.241	14.172
17LM01-8.1	0.231	0.222	0.510	2.221	3.645	9.506	20.908	41.388	87.440
17LM01-8.2	0.143	0.133	0.351	1.724	2.669	6.801	16.707	29.868	75.274
17LM01-9.1	0.157	0.199	0.384	1.954	3.486	10.385	25.515	23.900	22.225
17LM01-10.1	0.002	0.061	0.024	0.528	0.506	6.024	14.933	11.249	8.894
17LM01-11.1	0.137	0.183	0.422	1.906	3.082	9.583	14.956	11.243	10.772
17LM01-12.1	0.169	0.102	0.150	0.640	1.147	5.557	23.710	45.544	58.456
17LM01-13.1	0.085	0.114	0.137	0.946	1.603	7.168	17.585	15.064	11.588
17LM01-14.1	0.047	0.100	0.151	1.255	1.606	8.364	19.705	14.090	10.959
17LM01-15.1	1.058	0.495	0.709	2.379	5.402	9.295	22.035	31.465	46.150
17LM01-16.1	0.017	0.066	0.078	0.625	0.533	5.656	18.753	20.741	21.178
17LM01-17.1	0.055	0.060	0.142	0.385	1.051	1.119	5.651	37.815	158.581
17LM01-18.1	0.012	0.058	0.036	0.584	0.680	5.128	14.171	12.660	12.305
17LM01-19.1	0.261	0.293	0.709	2.831	4.590	9.832	20.993	35.208	90.636
17LM01-20.1	0.229	0.224	0.522	2.535	4.796	12.724	36.860	47.161	53.148
17LM01-21.1	0.168	0.269	0.431	2.892	4.605	22.567	47.420	32.452	21.225

17LM01-22.1	0.034	0.066	0.045	0.513	0.586	4.560	18.587	31.383	44.347
17LM01-23.1	0.036	0.088	0.091	0.707	0.961	6.023	13.553	12.562	11.958
17LM01-24.1	0.003	0.046	0.013	0.439	0.349	4.740	12.568	11.261	10.269
17LM01-25.1	0.000	0.054	0.019	0.518	0.433	5.887	13.011	10.552	10.374
17LM01-26.1	0.017	0.052	0.035	0.308	0.729	2.179	17.637	43.984	71.317
17LM01-27.1	0.070	0.100	0.163	0.985	1.426	6.520	17.378	18.314	18.998
17LM01-28.1	0.031	0.064	0.060	0.413	0.894	3.480	25.097	48.643	64.208
17LM01-29.1	0.042	0.117	0.135	0.756	1.399	5.748	26.528	53.089	92.026
17LM01-30.1	0.008	0.066	0.026	0.472	0.514	6.486	17.990	15.244	10.599

Table 3. Zircon trace element analyses for representative Ledge Mountain migmatites

FIGURES

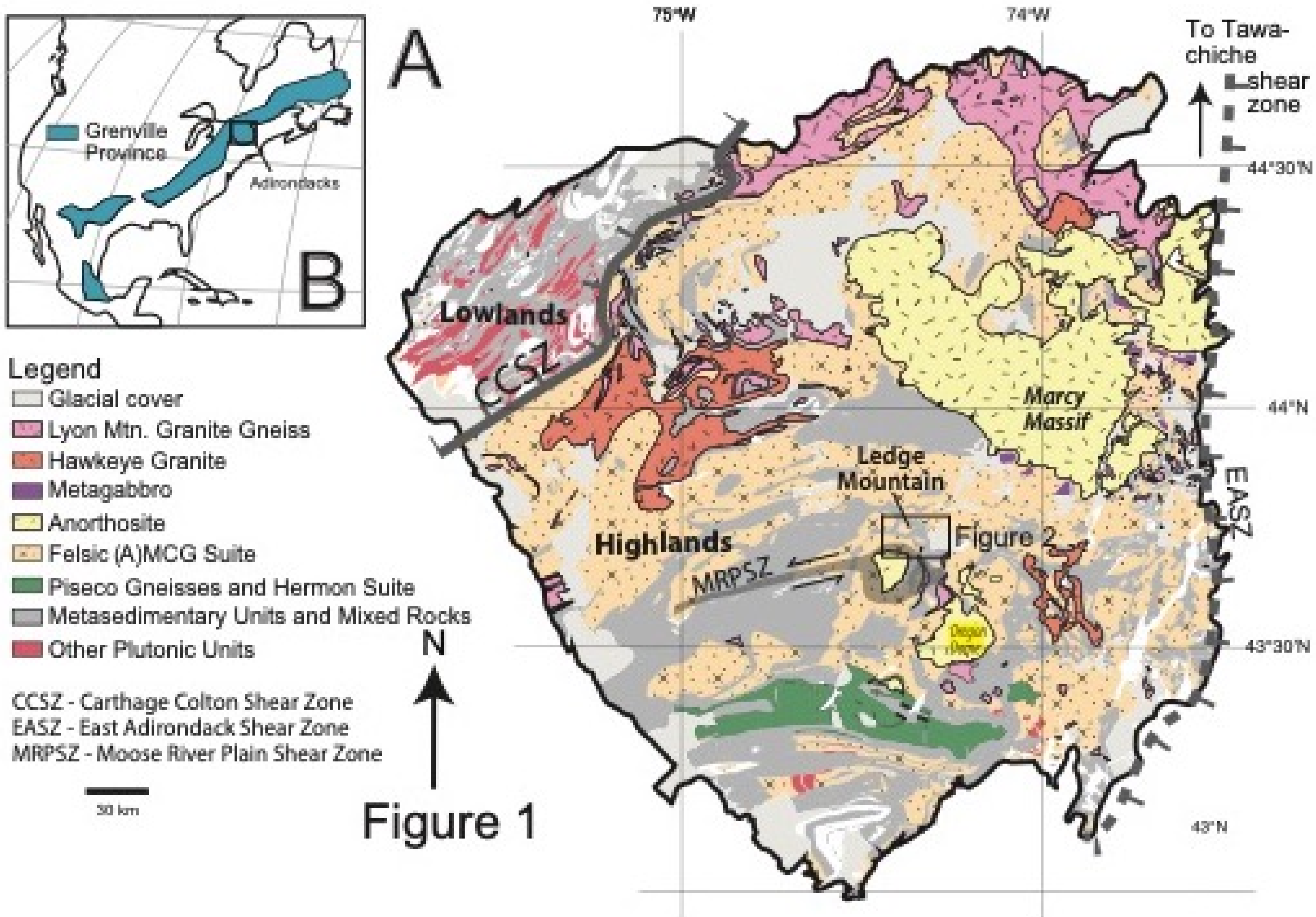

Figure 1

Figure 1. Geologic map of the Grenville orogenic belt and the Adirondack Mountains (modified from Wong et al., 2012 and Peck et al., 2013) A. General geologic map of major units, structures, and shear zones. B. Location of the Adirondacks within the North American Grenville orogen (after Rivers 1997, 2015). Square marks the extent of Figure 2.

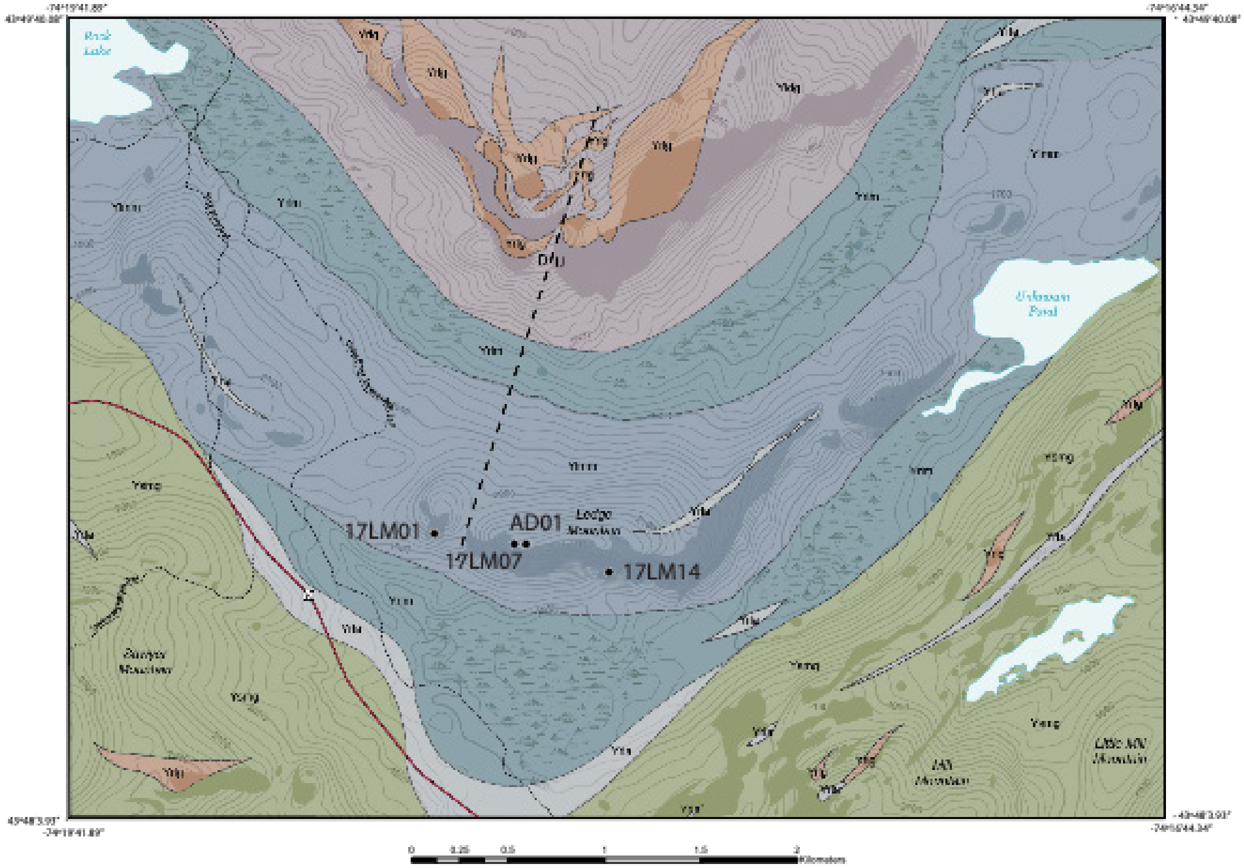

MAP SYMBOLS

17LM01 Sample location/no.

New York State Route 30

Trails

Contact between map units (Inferred)

Fault (Inferred)

Perennial lake/pond

Marsh

Contour Interval 20 ft

MN

13.6°

Yrlg — **Rock Lake gabbro**: This peak-forming metagabbro is non-foliated, characteristically gray to black, coarse-grained with a spotted appearance from weathered feldspar grains, and contains the assemblage: Pl ± Opx ± Cpx + Hbl ± Grt ± Bt + Opq (Fe-Ti oxides).

Ylmm — **Ledge Mountain Migmatites:** Ledge Mountain migmatites are a ridge-forming unit found along Ledge Mountain with the best exposures found on the steep cliff face on the southern side of Ledge Mountain.

Yrlm — **Rock Lake marble**: Geraghty (1978) identified marble in east-west-trending belts in topographic low areas between Stark Hills and Ledge Mountain, and to the south of Ledge Mountain.

Yldg — **Lake Durant gneiss**: The Lake Durant gneiss crops out in the Stark Hills area and consists of pink to tan, foliated, medium- to coarse-grained quartzofeldspathic gneiss interlayered with quartzite and amphibolite.

Yrla — **Rock Lake amphibolite**: Lenses of amphibolite are characteristically black, medium-grained amphibolite with the assemblage Hbl + Pl + Bt + Qz + Opq + Opx? ± Grt.

Ysmg — **Sawyer Mountain gneiss:** This unit is a white to gray quartzofeldspathic gneiss forming Sawyer Mountain and the northern slopes of Mill Mountain and Little Mill Mountain.

Figure 2

Figure 2. Geologic map of part of the Rock Lake Quadrangle centered around Ledge Mountain. Adapted from NY Rock Lake Quadrangle. The four sample (AD01, 17LM01, 17LM07, and 17LM14) locations are marked. Contour interval is 6.1m (20 feet). A larger map was created as part of a USGS EDMAP grant.


A
B
C
Melanosome
Pegmatitic
Leucosome
Melanosome
E
Melanosome
Pegmatitic
Leucosome
Melanosome

Figure 3

Figure 3. Field photos showing macroscopic features. (A) 30’-long outcrop near the bend between the western and eastern branches of Ledge Mountain. Outcrops show large-scale evidence of flow within the melt. (B) Migmatite sample taken from the wall in Fig. 3A. Interlayered melanosome and pegmatitic leucosome visible in hand sample that shows evidence of flow within the melt; (C) In-situ outcrop showing layering of pegmatitic leucosome and melanosome; (D) In-situ outcrop showing layering of pegmatitic leucosome and melanosome; (E) Close up of pegmatitic leucosome from Figure 3D; (F) In-situ outcrop showing layering of pegmatitic leucosome and melanosome.

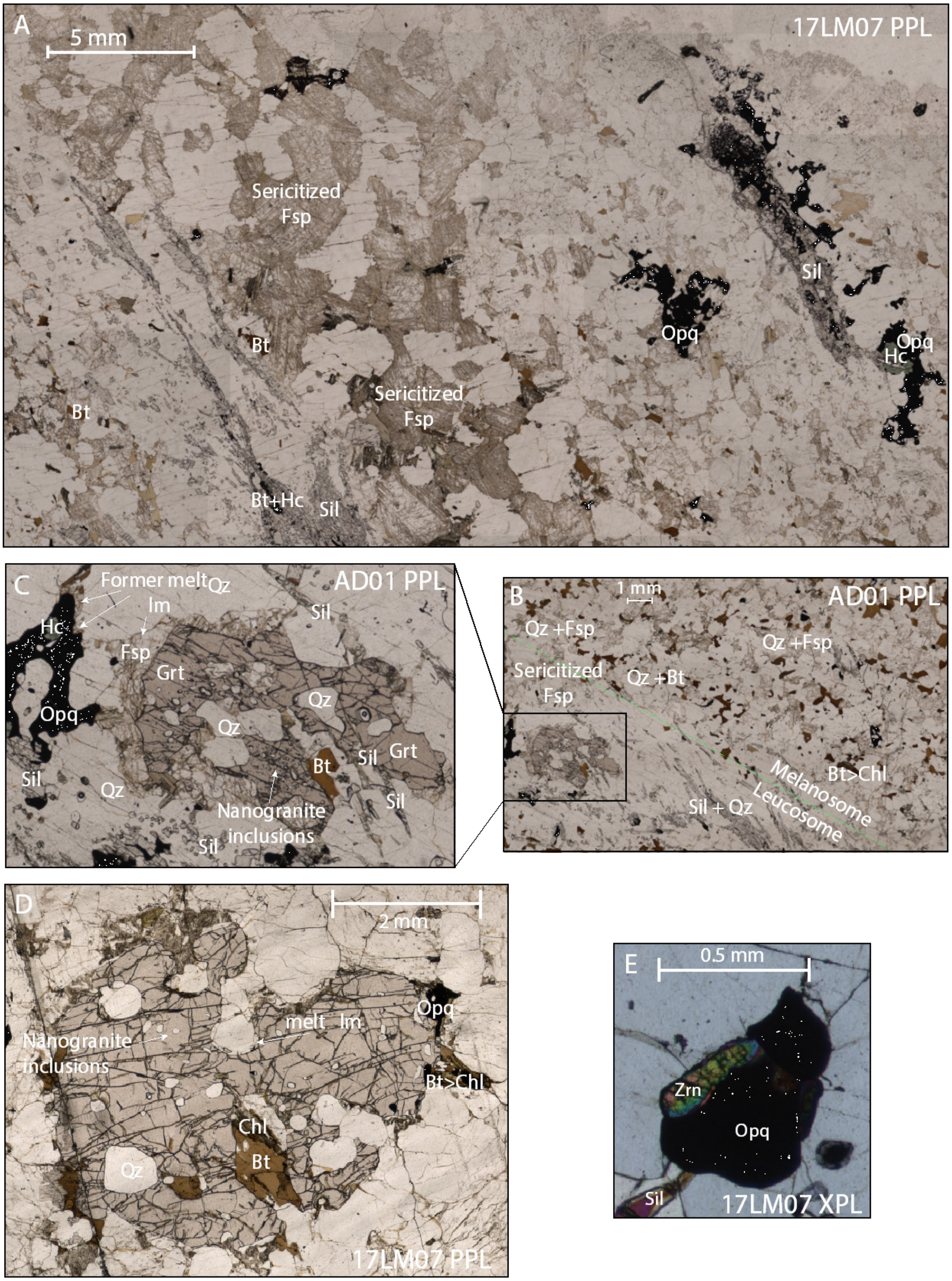
A
5 mm
17LM07 PPL
Sericitized
Fsp
Sil
Opq
Hc
Opq
Bt
Sericitized
Fsp
Bt
Bt+Hc
Sil
C
Former melt
Qz
AD01 PPL
Hc
Im
Sil
Fsp
Grt
Opq
Qz
Qz
Sil
Grt
Bt
Sil
Qz
Sil
Nanogranite
inclusions
Sil
B
1 mm
AD01 PPL
Qz +Fsp
Qz +Fsp
Sericitized
Fsp
Qz +Bt
Bt>Chl
Melanosome
Leucosome
Sil + Qz
D
2 mm
Opq
melt
Im
Nanogranite
inclusions
Bt>Chl
Chl
Bt
Qz
17LM07 PPL
E
0.5 mm
Zrn
Opq
Sil
17LM07 XPL

Figure 4

Figure 4. Photomicrographs showing the mineralogy and macro- and microtextures in Ledge Mountain migmatites. Mineral abbreviations are after Whitney and Evans (2010). (A) Part of a thin section scan of sample 17LM07 displaying aligned sillimanite (Sil) + quartz (Qz) + opaque minerals (Opq) in the leucosome. Evidence of retrogression in the sericitized feldspar (Fsp-Feldspar). Intergrown hercynite (Hc) and Fe-Ti oxides alongside Sil. (B) Part of a thin section scan of sample AD01 displaying melanosome with interlayered leucosome. Leucosome shows alignment of Sil + Qz and a peritectic garnet. Melanosome shows Qz + Fsp + Biotite (Bt). (C) Inset shows garnet in sample AD01 showing replacement feldspar (Fsp) + biotite (Bt) and relict garnet (broken off pieces). Nanogranite inclusions. Evidence of former melt as films of Fsp around Opq and Grt. (D) Peritectic garnet with late Bt. Former melt films in embayments in garnet. Chloritization of Bt. (E) Zircon grain along a Fe-Ti oxide.

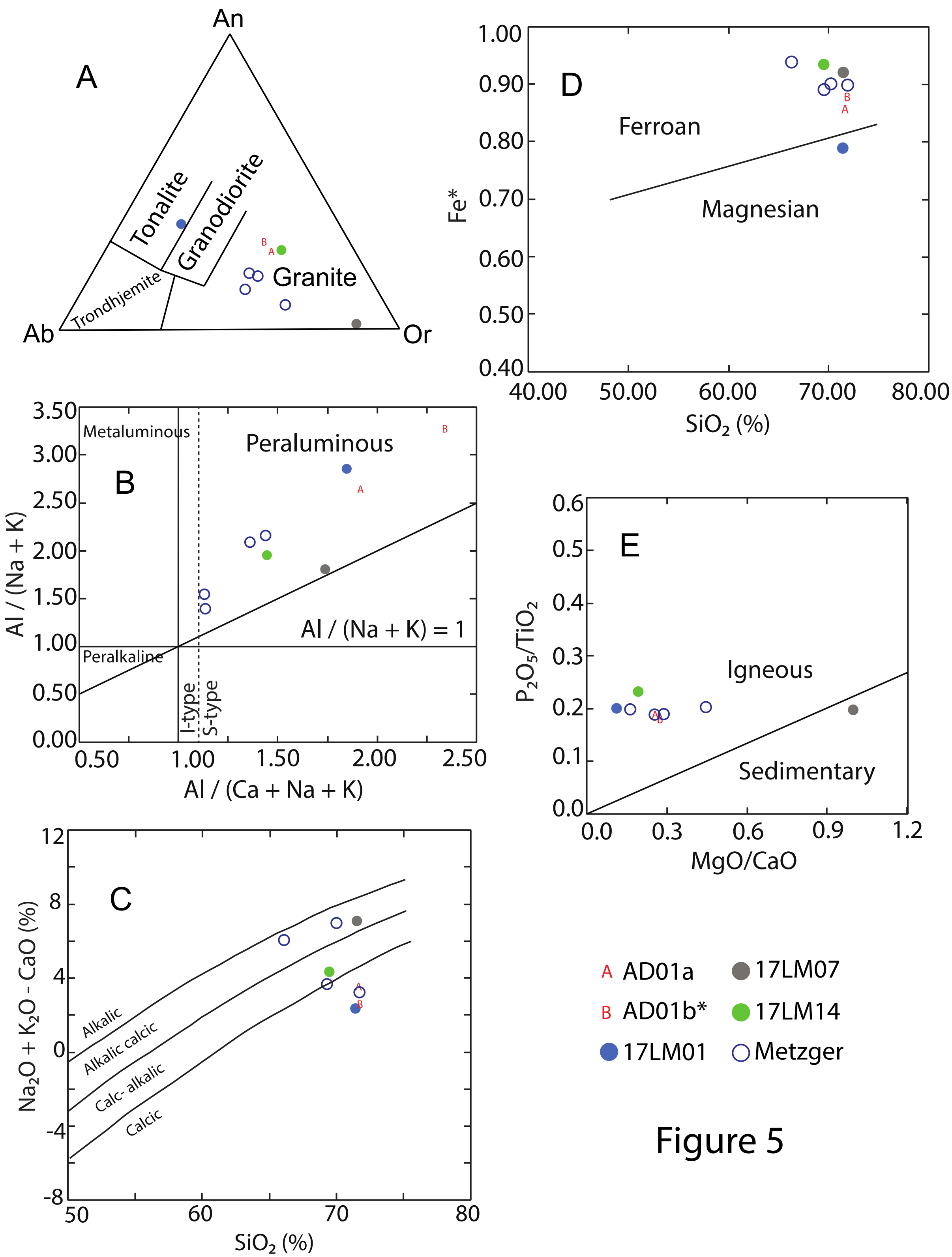
A
An
Ab
Or
Tonalite
Granodiorite
Trondhjemite
Granite
B
Metaluminous
Peraluminous
Peralkaline
Al / (Na + K) = 1
I-type
S-type
Al / (Na + K)
Al / (Ca + Na + K)
C
Alkalic
Alkalic calcic
Calc- alkalic
Calcic
Na2O + K2O - CaO (%)
SiO2 (%)
D
Ferroan
Magnesian
Fe*
SiO2 (%)
E
Igneous
Sedimentary
P2O5/TiO2
MgO/CaO
A AD01a
B AD01b*
17LM01
17LM07
17LM14
Metzger

Figure 5

Figure 5. Major element discrimination diagrams showing the modeled Ledge Mountain migmatites plotted with Ledge Mountain samples from Metzger. Whole rock data is used to identify traits from the samples. Two analyses were conducted on AD01 and are plotted separately as a red "A" and "B" corresponding with their whole rock data on Table 2. (A) Albite-anorthosite-orthoclase (Ab-An-Or) discrimination plot (Barker, 1979) showing that the Ledge Mountain samples, except for 17LM01, plot in the granite field. (B) Alumina index diagram (Manier and Piccoli, 1989) showing Ledge Mountain samples are peraluminous. (C) Modified alkali lime index [(Na_2O + K_2O - CaO) vs SiO_2]; Frost et al., 2001. Ledge Mountain samples plot in the alkali calcic to calcic fields. (D) Fe* versus SiO_2 (Frost and Frost, 2008), showing Ledge Mountain migmatites, except for 17LM01, fall in the ferroan field. Fe* = Fe/(Fe+Mg). (E) P_2O_5/TiO_2 versus MgO/CaO diagram to distinguish felsic orthogneiss from paragneiss protoliths, showing all Ledge Mountain samples. Sample 17LM07 narrowly falls in the sedimentary field (after Werner, 1987, cited in Ownby et al., 2004).

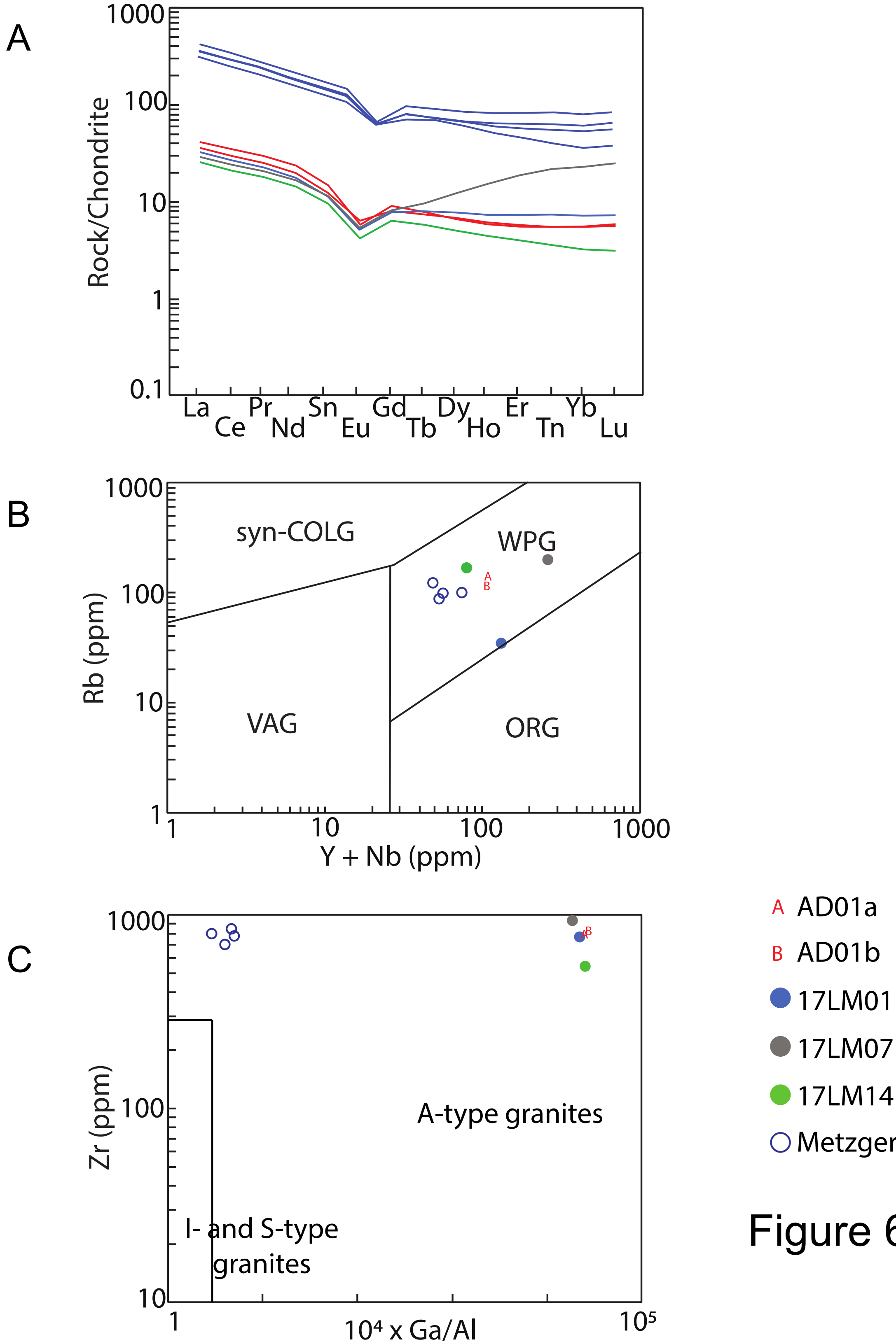

A
1000
100
10
1
0.1
Rock/Chondrite
La
Ce
Pr
Nd
Sn
Eu
Gd
Tb
Dy
Ho
Er
Tn
Yb
Lu
B
1000
100
10
1
syn-COLG
WPG
VAG
ORG
A
B
Rb (ppm)
1
10
100
1000
Y + Nb (ppm)
C
1000
100
10
Zr (ppm)
A-type granites
I- and S-type
granites
1
10^4 x Ga/Al
10^5
A AD01a
B AD01b
17LM01
17LM07
17LM14
Metzger

Figure 6

Figure 6. Trace element discrimination diagrams showing the modeled Ledge Mountain migmatites plotted with the Ledge Mountain samples from Metzger. Two analyses were conducted on AD01 and are plotted separately as a red “A” and “B” corresponding with their whole rock data on Table 2. (A) Chondrite-normalized spider diagram (McDonough and Sun, 1995). (B) Zr versus 10^4 x Ga/Al plot (Whalen et al., 1987) showing the modeled Ledge Mountain samples all plotted in the A-type granite field. (C) Rb versus Y + Nb discrimination plot (Pearce et al., 1984) showing the modeled LM samples plot in the within plate granite (WPG) field. ORG-ocean ridge granites; syn-COLG-syn-collisional granites; VAG-volcanic arc granites.

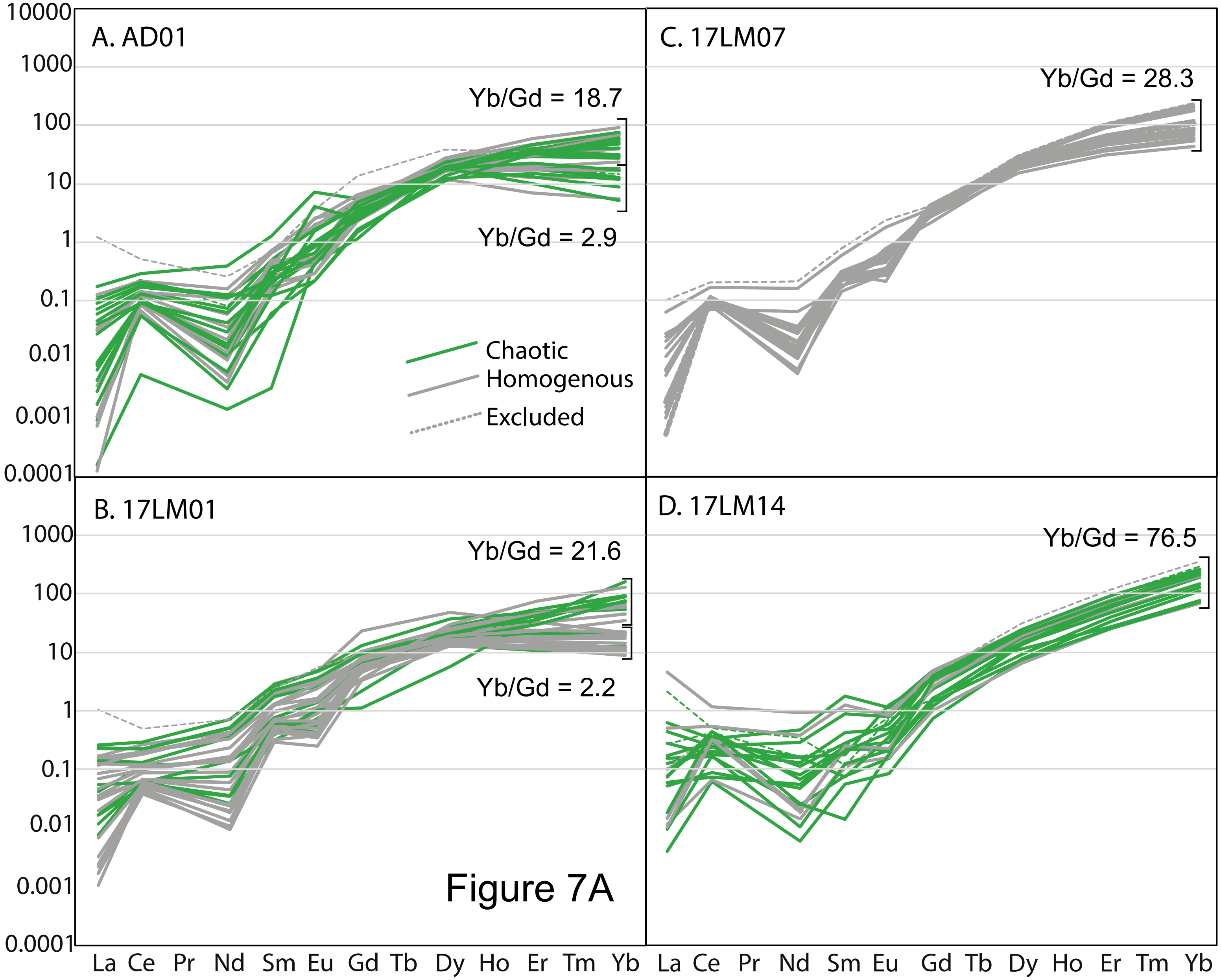
A. AD01
B. 17LM01
C. 17LM07
D. 17LM14
Yb/Gd = 18.7
Yb/Gd = 2.9
Yb/Gd = 21.6
Yb/Gd = 2.2
Yb/Gd = 28.3
Yb/Gd = 76.5
Chaotic
Homogenous
Excluded
10000
1000
100
10
1
0.1
0.01
0.001
0.0001
La Ce Pr Nd Sm Eu Gd Tb Dy Ho Er Tm Yb

Figure 7A

Figure 7A. Chondrite-normalized rare earth element spider diagram for the four migmatites samples. Normalization values are from McDonough and Sun (1995). Dashed lines represented zircon grains that have been excluded from SHRIMP analyses due to their discordant ages, see text for details. Green lines represent zircons with chaotic domains. Gray lines represent zircons with homogenous domains. All diagrams show a positive slope, trending from LREE to HREE, and weak Ce and Eu anomalies. HREE slopes are defined by Yb/Gd to show variable steep vs flat slopes which are labeled to show the two different populations found in same AD01 and 17LM01. Steep HREE slopes suggest zircons grew with plagioclase, at retrograde P-T conditions and flat HREE slopes suggest zircons grew in garnet-rich assemblages with garnet; this suggests different forms of metamorphism affected samples AD01 and 17LM01. (A) AD01 zircons show two populations in the HREE; those with an steep HREE slope (average Yb/Gd = 18.7) and those with a flat HREE slope (average Yb/Gd = 2.9). AD01 zircons show LREE concentrations varying on the order of 2+ magnitudes. (B) 17LM01 zircons show two populations in the HREE; those with an steep HREE slope (average Yb/Gd = 21.6) and those with a flat HREE slope (average Yb/Gd = 2.2). 17LM01 zircons show LREE concentrations varying on the order of 2 magnitude. (C) 17LM07 zircons show one population of elevated HREE with an average slope of Yb/Gd = 28.3. 17LM07 zircons show little variability in REE concentrations. (D) 17LM14 zircons show one population of elevated HREE with an average slope of Yb/Gd = 76.5. 17LM14 zircons show LREE concentrations varying on the order of 2 magnitude.

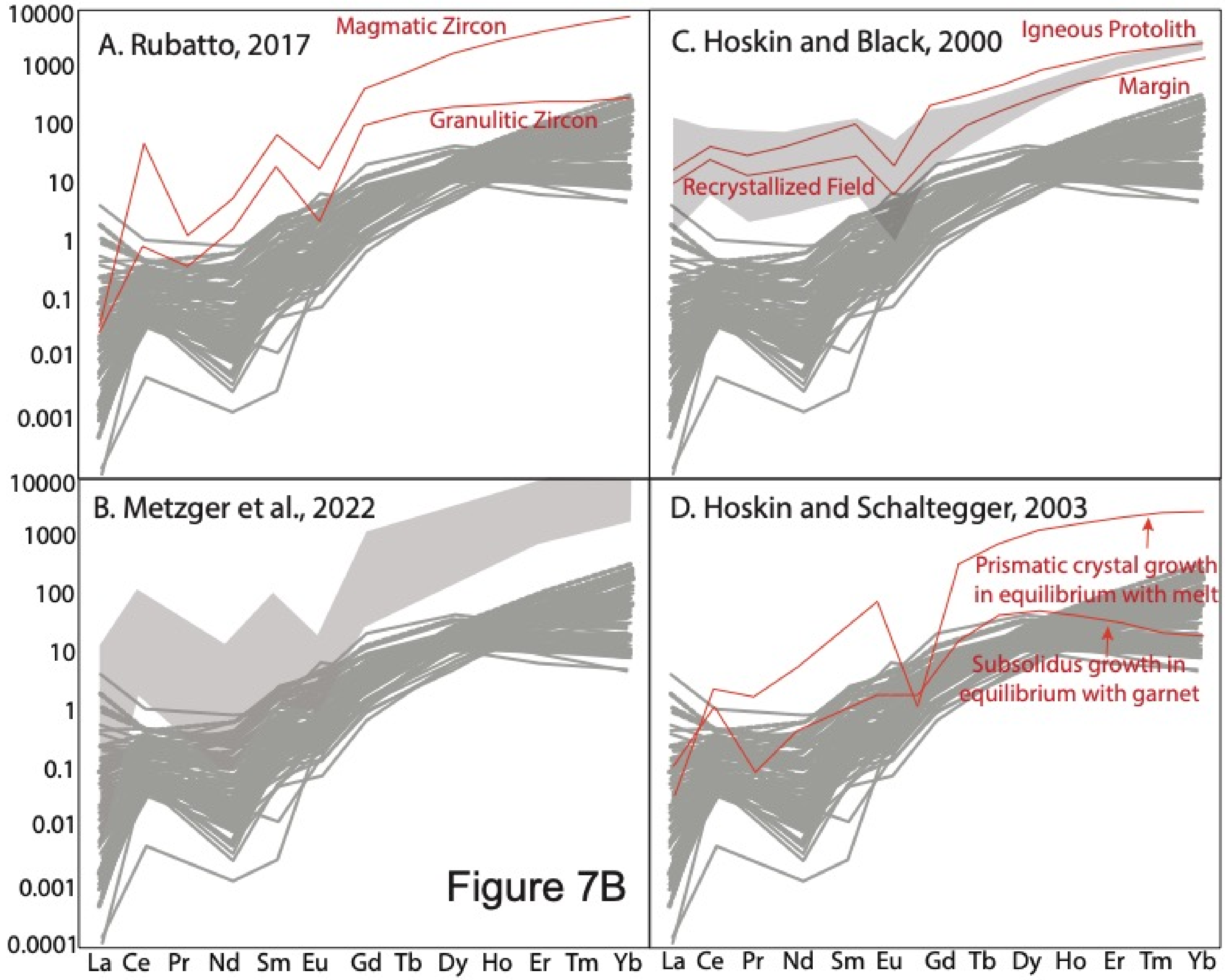
A. Rubatto, 2017
Magmatic Zircon
Granulitic Zircon
C. Hoskin and Black, 2000
Igneous Protolith
Margin
Recrystallized Field
B. Metzger et al., 2022
D. Hoskin and Schaltegger, 2003
Prismatic crystal growth in equilibrium with melt
Subsolidus growth in equilibrium with garnet
10000
1000
100
10
1
0.1
0.01
0.001
0.0001
La Ce Pr Nd Sm Eu Gd Tb Dy Ho Er Tm Yb
Figure 7B

Figure 7B. Zircon trace element spider diagrams are used to compare my zircons to modeled REE patterns from other researchers to make interpretations about metamorphism at Ledge Mountain. Normalization values are from McDonough and Sun (1995). Dashed lines represent zircon grains that have been excluded from SHRIMP analyses due to their discordant ages, see text for details. Green lines represent zircons with chaotic domains and gray lines represent zircons with homogeneous domains. (A) Zircon trace element spider diagrams compared to Rubatto (2017) show characteristic REE patterns for magmatic zircons and for granulitic zircons. My zircons show a REE pattern resembling the granulitic zircons with the weak Ce and Eu anomaly and a flatter HREE slope compared to the magmatic zircon. (B) Zircon trace element spider diagrams compared to Metzger et al., 2022. Gray field shows Metzger et al. (2022) samples that show HREE enrichment and unlike my zircons, lack a depleted HREE populations. (C) Zircon trace element spider diagrams compared to Hoskin and Black (2000) show gray fields of recrystallized zircons. The variation in LREE concentrations is explained by zircon's "memory" of its protolith. The variability in my zircon LREE concentrations can also be explained as protolith "memory". (D) Zircon trace element spider diagrams compared to Hoskin and Schaltegger (2003) and show a REE model of prismatic crystal growth in equilibrium with melt and a REE pattern for subsolidus growth in equilibrium with garnet. The populations of HREE depleted zircons in AD01 and 17LM01 resemble this subsolidus growth pattern suggesting solid-state metamorphism.

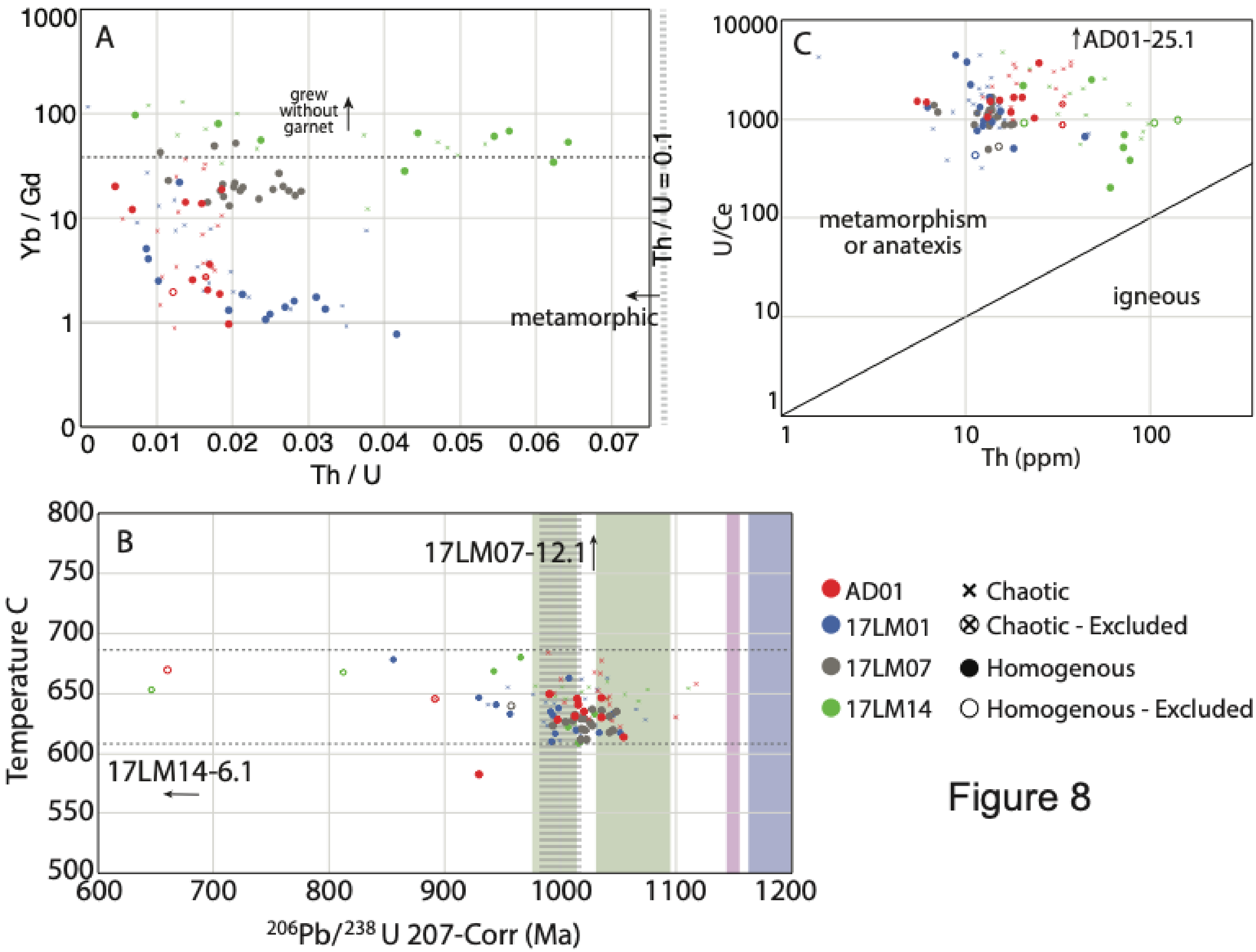

A
grew
without
garnet
metamorphic
Th / U = 0.1
Yb / Gd
Th / U
C
AD01-25.1
metamorphism
or anatexis
igneous
U/Ce
Th (ppm)
B
17LM07-12.1
17LM14-6.1
Temperature C
$^{206}Pb/^{238}U$ 207-Corr (Ma)
AD01
17LM01
17LM07
17LM14
Chaotic
Chaotic - Excluded
Homogenous
Homogenous - Excluded

Figure 8

Figure 8. Trace element discrimination diagrams showing the modeled Ledge Mountain migmatites plotted. Zircons with chaotic domains are marked with X and zircons with homogenous domains are marked with circles. (A) Plot of Yb/Gd versus Th/U ratios for all zircons. Th/U ratios <0.1 represent metamorphic settings; higher Th/U ratios indicate magmatic growth. Garnet preferentially incorporates heavy rare earth elements, so Yb/Gd ratios > 40 result from growth without garnet; most Ottawan-aged zircons have Yb/Gd > 40 and so likely grew post-peak metamorphism. (B) Ti-in-zircon temperatures versus age for all zircons except 17LM07-12.1 (855.5°C at 1029 Ma) and 17LM14-6.1 (664.1°C at 560 Ma). (C) Plot of U/Ce ratios versus Th (ppm) concentrations for all zircons. Plot includes all zircons except AD01-25.1 (U/Ce = 60,026.2), see Table 3. High U/Ce values indicate zircon growth in a metamorphic or anatectic setting, while low U/Ce values indicate magmatic zircon growth. All zircons fall within the metamorphism or anatexis field.

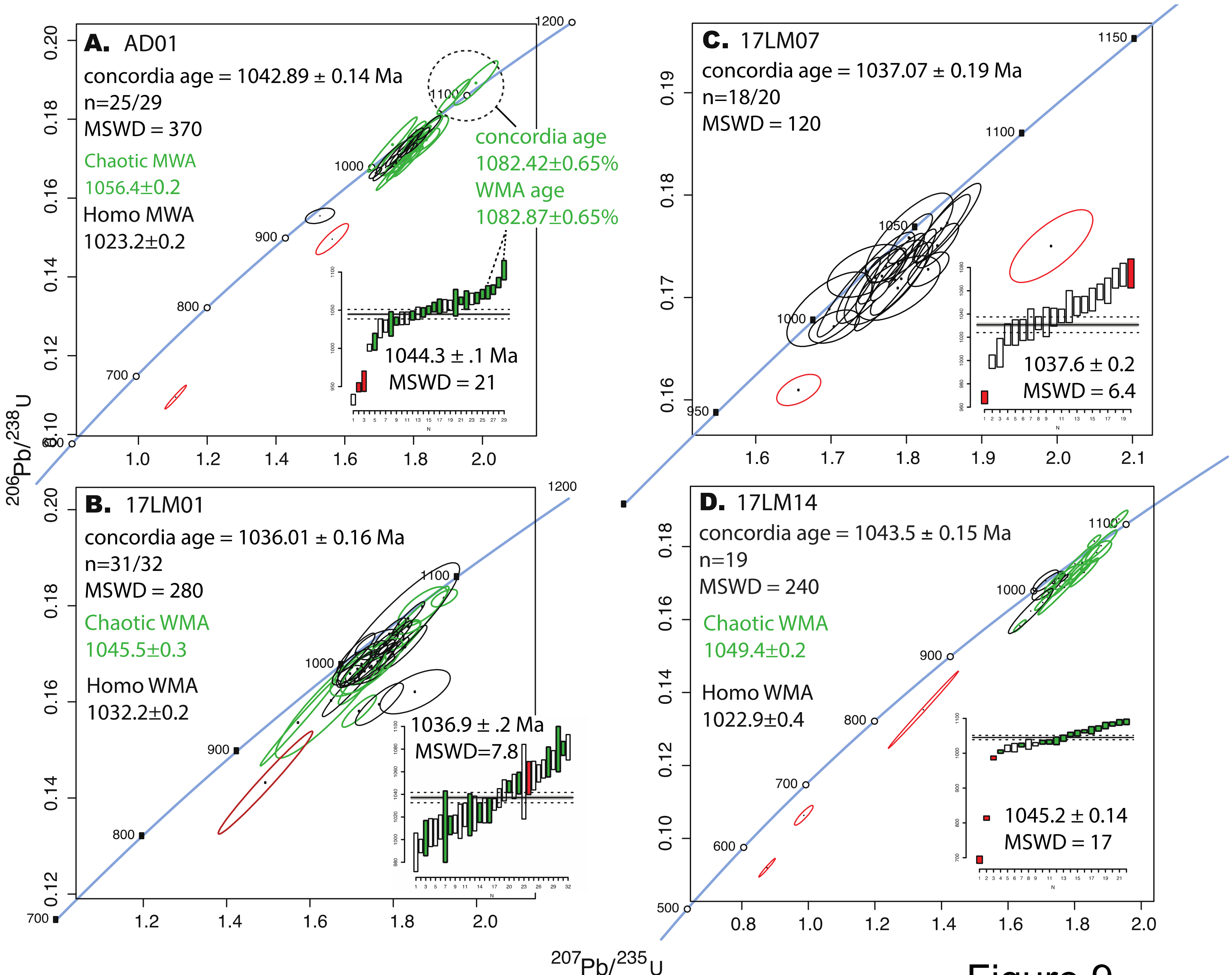
A. AD01
concordia age = 1042.89 ± 0.14 Ma
n=25/29
MSWD = 370
Chaotic MWA
1056.4±0.2
Homo MWA
1023.2±0.2
concordia age
1082.42±0.65%
WMA age
1082.87±0.65%
1044.3 ± .1 Ma
MSWD = 21
B. 17LM01
concordia age = 1036.01 ± 0.16 Ma
n=31/32
MSWD = 280
Chaotic WMA
1045.5±0.3
Homo WMA
1032.2±0.2
1036.9 ± .2 Ma
MSWD=7.8
C. 17LM07
concordia age = 1037.07 ± 0.19 Ma
n=18/20
MSWD = 120
1037.6 ± 0.2
MSWD = 6.4
D. 17LM14
concordia age = 1043.5 ± 0.15 Ma
n=19
MSWD = 240
Chaotic WMA
1049.4±0.2
Homo WMA
1022.9±0.4
1045.2 ± 0.14
MSWD = 17
$^{206}Pb/^{238}U$
$^{207}Pb/^{235}U$

Figure 9

Figure 9. Concordia diagrams and weighted mean age diagrams for all U-Pb sensitive high-resolution ion microprobe (SHRIMP) analysis of zircons from samples AD01, 17LM01, 17LM07, and 17LM14 corresponding to the data in Table 4. Green ellipses on the concordia plots and green rectangles in the WMA plots represent zircons with chaotic domains. Black ellipses and rectangles represent zircons with homogenous domains. (A) Sample AD01 gave one concordant analysis (1044.27 ± 0.13 Ma) excluding two discordant zircons in red, AD01-2.1, with an age of 660.33 ± 11.69 Ma, and AD01-24.1, with an age of 891.36 ± 15.00 Ma. The calculated weighted mean age for all AD01 zircons is 1045.7 ± 0.1 Ma excluding AD01-2.1 and AD01-24.1. The calculated weighted mean age for chaotic zircons is 1056.4 ± 0.2 Ma. The calculated weighted mean age for homogenous zircons is 1023.2 ± 0.2 Ma. (B) Sample 17LM01 gave one concordant analysis (1036.01 ± 0.16 Ma) excluding one discordant zircon in red, 17LM01-15.1, with an age of 855.92 ± 40.67 Ma. The calculated weighted mean age is 1036.9 ± 0.2 Ma excluding 17LM01-15.1. The calculated weighted mean age for chaotic zircons is 1045.5 ± 0.3 Ma. The calculated weighted mean age for homogenous zircons is 1032.2 ± 0.2 Ma. (C) Sample 17LM07 gave one concordant analysis (1037.07 ± 0.19 Ma) excluding two discordant zircons in red, 17LM07-9.1, with an age of 958.63 ± 5.78, and 17LM07-12.1, with an age of 1028.98 ± 13.23 Ma. The calculated weighted mean age is 1037.6 ± 0.2 Ma excluding 17LM07-9.1 and 17LM07-12.1. All zircons from 17LM07 are homogenous. (D) Sample 17LM14 gave one concordant analysis (1043.5 ± 0.15 Ma) excluding three discordant zircons in red, 17LM14-6.1 (560.38 ± 10.03 Ma), 17LM14-9.1 (812.43 ± 40.55 Ma) and 17LM14-10.1 (646.86 ± 10.56 Ma). The calculated weighted mean age is 1045.2 ± 0.14 Ma. The calculated weighted mean age for chaotic zircons is 1049.4 ± 0.2 Ma. The calculated weighted mean age for homogenous zircons is 1022.9 ± 0.4 Ma.

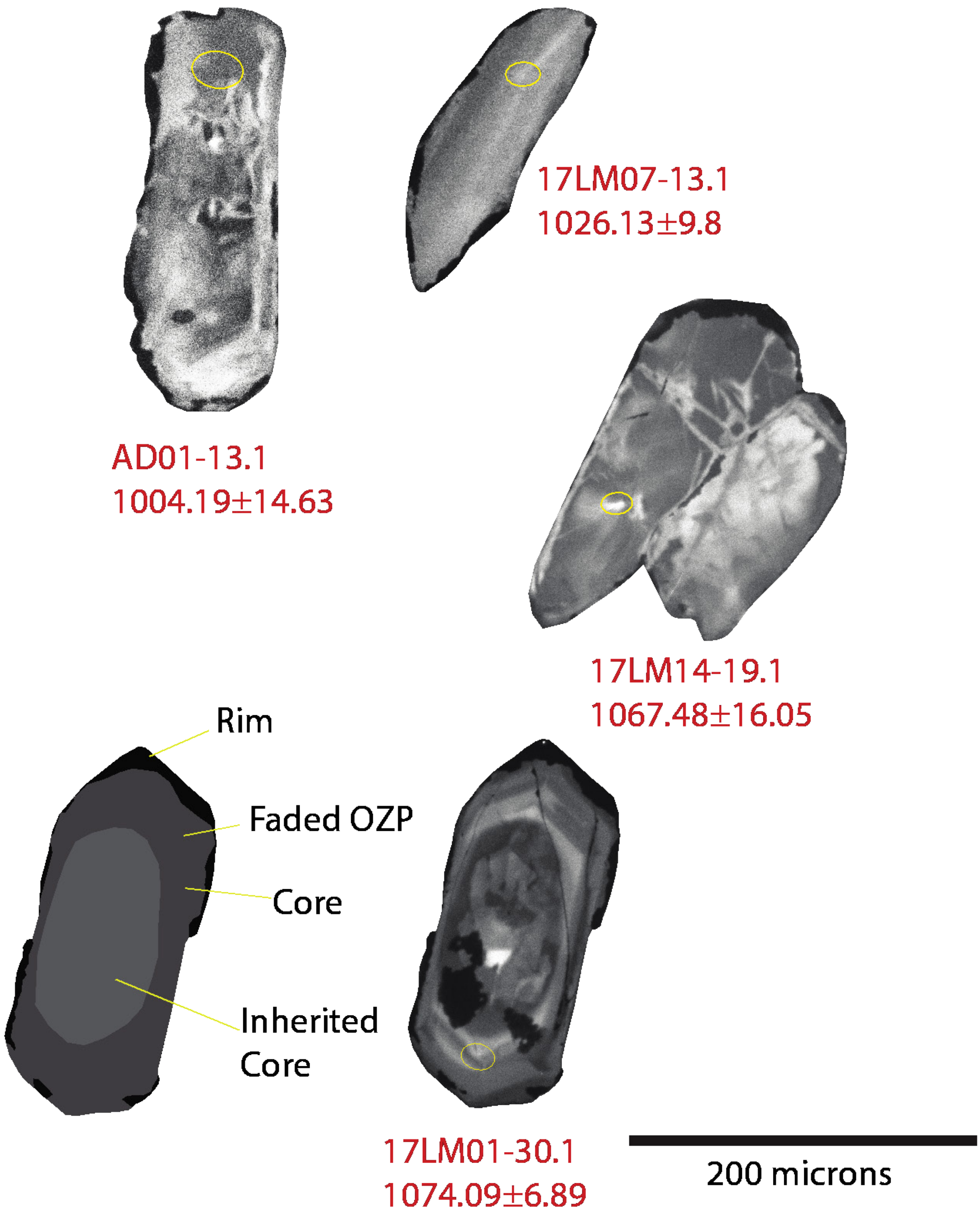
AD01-13.1
1004.19±14.63
17LM07-13.1
1026.13±9.8
17LM14-19.1
1067.48±16.05
Rim
Faded OZP
Core
Inherited
Core
17LM01-30.1
1074.09±6.89
200 microns

Figure 10A

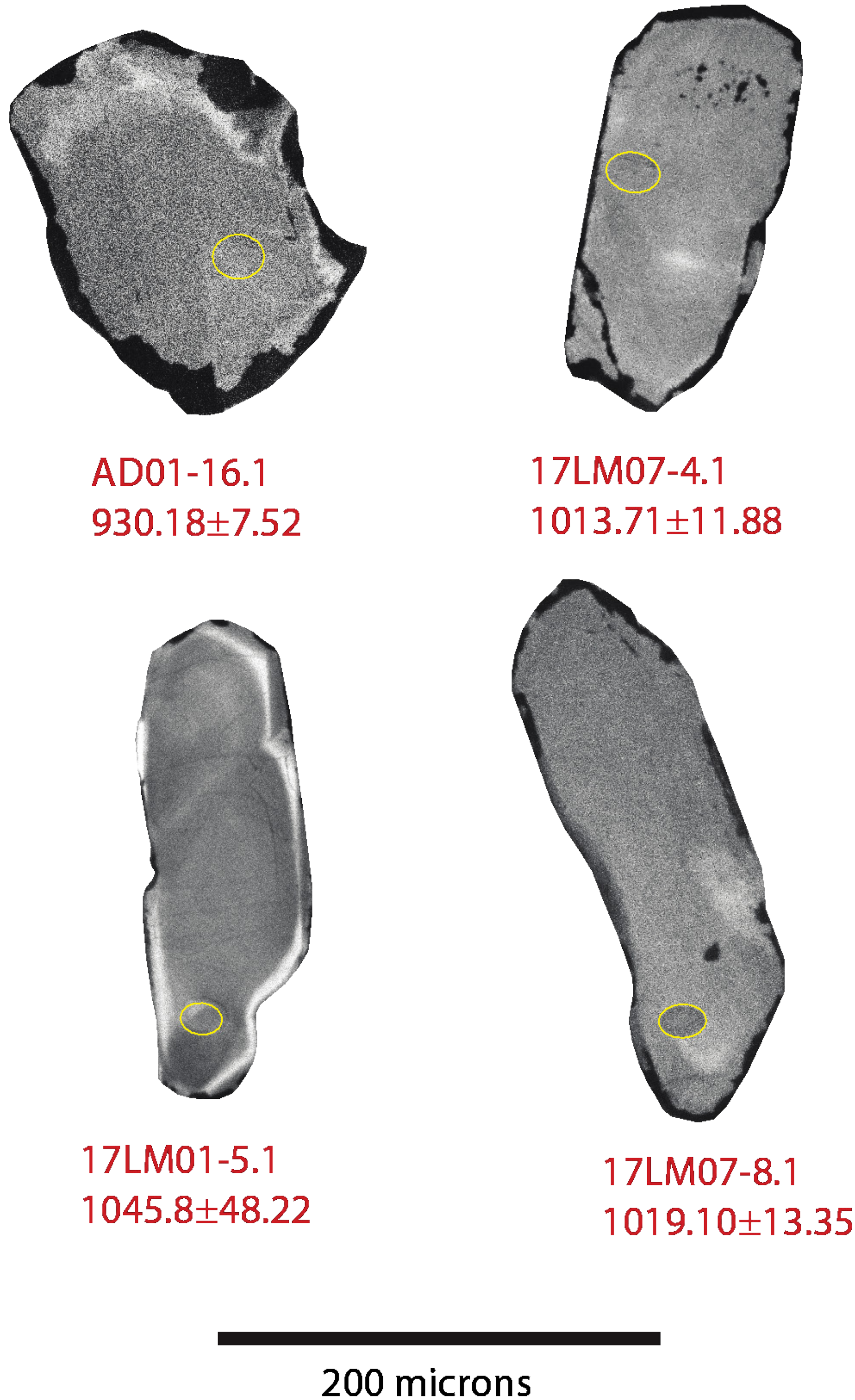
AD01-16.1
930.18±7.52
17LM07-4.1
1013.71±11.88
17LM01-5.1
1045.8±48.22
17LM07-8.1
1019.10±13.35
200 microns

Figure 10B

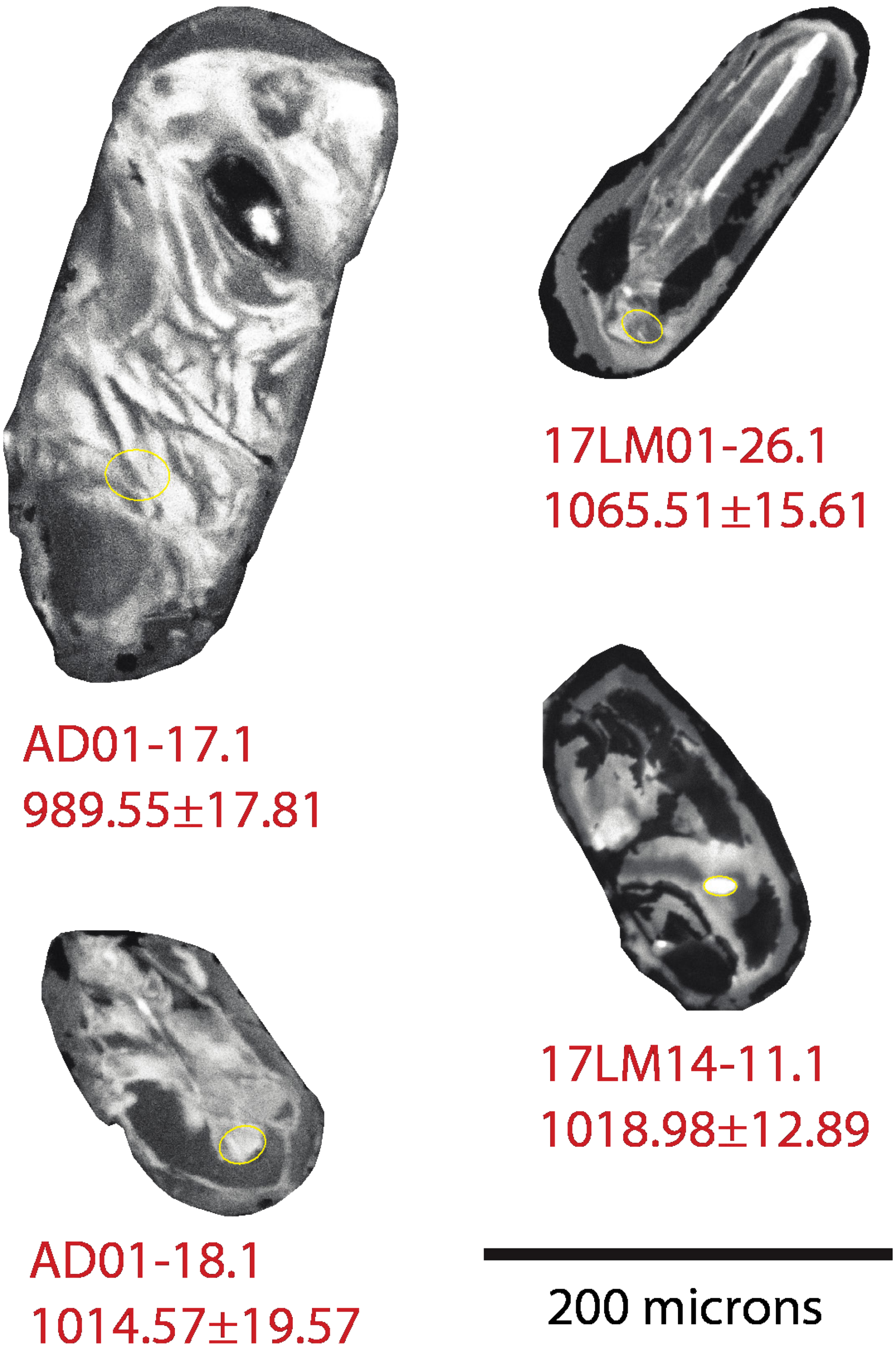
17LM01-26.1
1065.51±15.61
AD01-17.1
989.55±17.81
17LM14-11.1
1018.98±12.89
AD01-18.1
1014.57±19.57
200 microns

Figure 10C

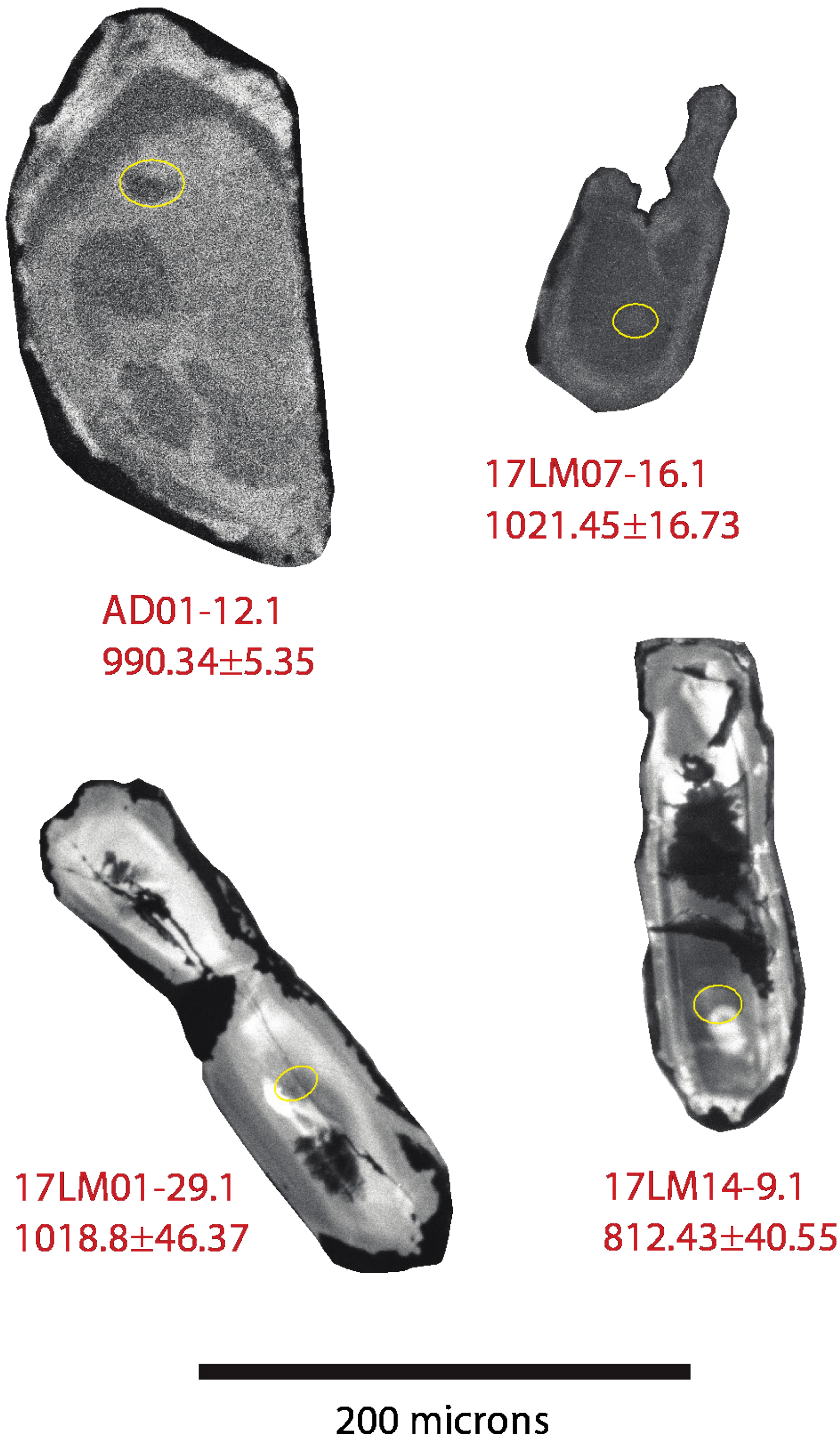
17LM07-16.1
1021.45±16.73
AD01-12.1
990.34±5.35
17LM01-29.1
1018.8±46.37
17LM14-9.1
812.43±40.55
200 microns

Figure 10D

Figure 10A-D. Cathodoluminescence (CL) imaging of zircons dated by U-Th-Pb sensitive high-resolution ion microprobe (SHRIMP) geochronology for samples of melanosome with microscopically interlayered leucosome and pegmatitic leucosome. Sample numbers and spot names corresponding to Table 4 are shown with ages ± 1σ errors (in Ma). Samples AD01, 17LM07, and 17LM14 are melanosome with microscopically interlayered leucosome. 17LM01 is a pegmatitic leucosome. (A) Representative zircons for each of the four rock samples are shown to give an overall idea of zircons from each rock sample. (B) Examples of homogenous zircons that display a limited range of CL brightnesses from bright to medium bright. (C) Examples of chaotic zircons that display a range of CL brightnesses from bright to dark and irregular patterns throughout the core domain. (D) Examples of zircons featuring faded oscillatory patterns which are evidence of solid-state recrystallization.

REFERENCES CITED

Aleinikoff, J.N., Walsh, G., and McAleer, R.J., 2021, New interpretations of the ages of origins of the Hawkeye Granite Gneiss and Lyon Mountain Granite Gneiss, Adirondack Mountains, NY: Implications for the nature and timing of Mesoproterozoic plutonism, metamorphism, and deformation

Baird, G.B., 2020, Late Ottawan orogenic collapse of the Adirondacks in the Grenville province of New York State: Integrated petrologic, geochronologic, and structural analysis of the Diana Complex in the southern Carthage-Colton mylonite zone: Geosphere, v. 16, p. 844-874

Barth, A.P., and Wooden, J.L., 2010, Coupled elemental and isotopic analyses of polygenetic zircons from granitic rocks by ion microprobe, with implications for melt evolution and the source of granitic magmas: Chemical Geology, v. 277, p. 149–159, https://doi.org/10.1016/j.chemgeo.2010.07.017.

Black, L.P., Kamo, S.L., Allen, C.M., Davis, D.W., Aleinikoff, J.N., Valley, J.W., Mundil, R., Campbell, I.H., Korsch, R.J., Williams, I.S., and Foudoulis, C., 2004, Improved $^{206}Pb/^{238}U$ microprobe geochronology by the monitoring of a trace-element-related matrix effect; SHRIMP, ID–TIMS, ELA–ICP–MS and oxygen isotope documentation for a series of zircon standards: Chemical Geology, v. 205, p. 115–140, https://doi.org/10.1016/j.chemgeo.2004.01.003.

Bohlen, S.R., Essene, E.J., and Hoffman, K.S., 1980, Update on feldspar and oxide thermometry in the Adirondack Mountains, New York: ecological Society of America Bulletin, v. 91, p. 110-113, https://dio.org/10.1130/0016-7606(1980)91<110:UOFAOT>2.0.CO;2

Bohlen, S.R., Valley, J.W., and Essene, E.J., 1985, Metamorphism in the Adirondacks, I. Petrology, Temperature, and Pressure: Journal of Petrology, v. 26, p. 971-992.

Bohlen, S.R., and Essene, E.J., 1977, Feldspar and oxide thermometry of granulites in the Adirondack Highlands: Contributions to Mineralogy and Petrology, v. 62, p.153-169.

Bickford, M.E., McLelland, J.M., Selleck, B.W., Hill, B.M., and Heumann, M.J., 2008, Timing of anatexis in the eastern Adirondack Highlands: Implications for tectonic evolution during ca. 1050 Ma Ottawan orogenesis: Geological Society of America Bulletin, v. 120, p. 950-961, https://doi.org/10.1130/B26309.1.

Chen, R.X, and Zheng, Y.F., 2017, Metamorphic zirconology of continental subduction zones: Journal of Asian Earth Sciences, v. 145, p. 149-176. http://dx.doi.org/10/1016/j.jseaes.2017.04.029

Chiarenzelli, J., Selleck, B., Lupulescu, M., Regan, S., Bickford, M.E., Valley, P., and McLelland, J., 2017, Lyon Mountain ferroan leucogranite suite: Magmatic response to extensional thinning of over thickened crust in the core of the Grenville orogen: Geological Society of America Bulletin, v. 129, p. 1472-1488, https://doi.org/10.1130/B31697.1.

Coble, M.A., Vazquez, J., Barth, A.P., Wooden, J., Burns, D., Kylander-Clark, A., Jackson, S., and Vennari, C.E., 2018, Trace element characterization of MAD-559 zircon reference material for ion microprobe analysis: Geostandards and Geoanalytical Research, v. 42, p. 481-497, https://doi.org/10.1111/ggr.12238.

Corfu, F., Hanchar, J.M., Hoskin, P.W.O, and Kinny, P., 2003, Atlas of zircon textures: Reviews in Mineralogy and Geochemistry, v. 53, p. 469-500. https://doi.org/10.2113/0530469.

Frost, B.R., Barnes, C.G., Collins, W.J., Arculus, R.J., Ellis, D.J., and Frost C.D., 2001, A geochemical classification for granitic rocks: Journal of Petrology, v. 42, p. 2033-2048, https://doi.org/10.1093/petrology/42.11.2033.

Frost, B.R., and Frost, C.D., 2008, A geochemical classification for feldspathic igneous rocks: Journal of Petrology, v. 49, p. 1955-1969, https://doi.org/10.1093/petrology/egn054.

Florence, F.P., and Spear, F.S., 1995, Intergranular diffusion kinetics of Fe and Mg during retrograde metamorphism of a pelitic gneiss from the Adirondack Mountains: Earth and Planetary Science Letters, v. 134, p. 329-340.

Geraghty, E.P., 1978, Structure, stratigraphy, and petrology of part of the Blue Mountain 15' quadrangle, central Adirondack Mountains, New York [Ph.D. thesis]: Syracuse, New York, Syracuse University, 281 p.

Grant, N., Lepak, R., Maher, T., Hudson M., and Carl, J., 1986, Geochronological framework of the Grenville Province of the Adirondack Mountains: Geological Society of America Abstracts with Programs, v. 18, p. 620: in McLelland, J., and Chiarenzelli, J., 1988, U-Pb zircon geochronology of the Adirondack Mountains and implications for their geologic evolution: Geology, v. 16, p. 920-924

Grimes, C.B., Wooden, J.L., Cheadle, M.J., and John, B.E., 2015, "Fingerprinting" tectono-magmatic provenance using trace elements in igneous zircon: Contributions to Mineralogy and Petrology, v. 170.

Hacker, B.R., Ratschbacher, L., Webb, L., Ireland, T., Walker, D., and Shuwen, D., 1998, U/Pb zircon ages constrain the architecture of the ultrahigh-pressure Qinling-Dabie Orogen, China: Earth and Planetary Science Letters, v. 161, p. 215-230

Hamilton, M.A., McLelland, J., and Selleck, B., 2004, SHRIMP U-Pb zircon geochronology of the anorthosite- mangerite-charnockite-granite suite, Adirondack Mountains, New York: Ages of emplacement and metamorphism, in Tollo, R.P., Corriveau, L., McLelland, J.M., and Barholomew, M.J., eds., Proterozoic Tectonic Evolution of the Grenville Orogen in

North America: Geological Society of America Memoir, v. 197, p. 337-355, https://doi.org/10.1130/0-8137-1197-5.337

Harley, S.L., 2004, Extending our understanding of ultrahigh temperature crustal metamorphism: Journal of Mineralogical and Petrological Sciences, v. 99, p. 140–158, https://doi.org/10.2465/jmps.99.140.

Hoskin, P.W.O., 2000, Patterns of chaos: fractal statistics and the oscillatory chemistry of zircon: Ceochimica et Cosmochimica Acta, v. 64, p. 1905-1923, doi:10.1016/S0016-7037(00)00330-6

Hoskin, P.W.O., and Black, L.P., 2000, Metamorphic zircon formation by solid-state recrystallization of protolith igneous zircon: Journal of Metamorphic Geology, v. 18, p. 423-439, https://doi.org/10.1046/j.1525-1314.2000.00266.x

Hoskin, P.W.O., and Schaltegger, U., 2003, The composition of zircon and igneous and metamorphic petrogenesis: Reviews in Mineralogy and Geochemistry, v. 53, p. 27-62, https://doi.org/10.2113/0530027.

Ireland, T.R., and Williams, I.S., 2003, Considerations in Zircon Geochronology by SIMS: Reviews in Mineralogy and Geochemistry, v. 53, p. 215-241, https://doi.org/10.2113/0530215.

Kelsey, D.E., Clark, C., and Hand, M., 2008, Thermobarometric modelling of zircon and monazite growth in melt-bearing systems: Examples using model metapelitic and metapsammitic granulites: Journal of Metamorphic Geology, v. 26, p. 199–212, https://doi.org/10.1111/j.1525-1314.2007.00757.x.

Lasalle, S., and Indares, A., 2014, Anatectic record and contrasting P-T paths of aluminous gneisses from the central Grenville Province: Journal of Metamorphic Geology, v. 32, p. 627-646.

Ludwig, K.R., 2009, Squid 2, A user's manual: Berkeley Geochronology Center Special Publication 5, 110 p.

Ludwig, K.R., 2012, User's manual for Isoplot 3.75: A geochronological toolkit for Microsoft Excel, Berkeley Geochronology Center Special Publication 5, 75 p.

McDonough, W.F. and Sun, S.S., 1995, The composition of the Earth: Chemical geology, v. 120, p. 223-253.

McLelland, J., Chiarenzelli, J., Whitney, P., and Isachsen, Y., 1988, U-Pb zircon geochronology of the Adirondack Mountains and implications for their geologic evolution, Geology, v. 16, p. 920-924.

McLelland, J.M., and Chiarenzelli, J., 1990, Isotopic Constraints on Emplacement age of anorthositic rocks of the marcy massif, Adirondack Mountains, NY

McLelland, J., Daly, J.S., and McLelland, J.M., 1996, The Grenville Orogenic Cycle (ca. 1350-1000 Ma): an Adirondack perspective: Tectonophysics, v. 265, p. 1-28.

McLelland, J.M., Bickford, M.E., Hill, B.M., Clechenko, C.C., Valley, J.W., and Hamilton, M.A., 2004, Direct dating of Adirondack massif anorthosite by U-Pb SHRIMP analysis of igneous zircon: Implications for AMCG complexes: Geological Society of America Bulletin, v. 116, p. 1299-1317, https://doi.org/10.1130/B25482.1.

McLelland, J.M., Selleck, B.W., and Bickford, M.E., 2010, Review of the Proterozoic Evolution of the Grenville province, its Adirondack outlier, and the Mesoproterozoic inliers of the Appalachians: Geoscience Canada, v. 40, p. 318-352.

McLelland, J.M., and Selleck, B.W., 2011, Megacrystic Gore Mountain–type garnets in the Adirondack Highlands: Age, origin, and tectonic implications. Geosphere, v. 7, p. 1194-1208.

McLelland, J. M., Selleck, B.W., and Bickford, M.E., 2013, Tectonic Evolution of the Adirondack Mountains and Grenville Orogen Inliers within the USA: Geoscience Canada, v. 40, p. 318-352.

Metzger, E.P., Leech, M.L., Davis, M.W., Reeder, J.V., Swanson, B.A., and Waring, H.V., 2022, Ultrahigh-temperature granulite-facies metamorphism and exhumation of deep crust in a migmatite dome during late- to post- orogenic collapse and extension in the central Adirondack Highlands: Geosphere, v. 18 (1), p. 261-297

Ownby, S.E., Miller, C.F., Berquist, P.J., Carrigan, C.W., Wooden, J.L., and Fullager, P.D., 2004, U-Pb geochronology and geochemistry of a portion of the Mars Hill terrance, North Carolina-Tennessee: Constraints on origin, history and tectonic assembly, in Tollo, R.P., Corriveau, L., McLelland, J.M., and Bartholomew, M.J., eds., Proterozoic Tectonic Evolution of the Grenville Orogen in North America: Geological Society of America Memoir, v. 197, p. 609-632

Pearce, J.A., Harris, N.B., and Tindle, A.G., 1984, Trace element discrimination diagrams for the tectonic interpretation of granitic rocks: Journal of Petrology, v. 25, p. 956-983, https://doi.org/10.1093/petrology/25.4.956

Peck, W.H., Selleck, B.W., Wong, M.S., Chiarenzelli, J.R., Harpp, K.S., Hollocher, K., Lackey, J.S., Catalano, J., Regan, S.P., and Stocker, A., 2013, Orogenic to postorogenic (1.20-1.15 Ga) magmatism in the Adirondack Lowlands and Frontenac terrane, southern

Grenville Province, USA and Canada: Geosphere, v. 9, p. 1637-1663, https://doi.org/10.1130/GES00879.1

Peck, W.H., Selleck, B.W., Regan, S.P., Howard, G.E., and Kozel, O.O., 2018, In-situ dating of metamorphism in Adirondack anorthosite: American Mineralogist, v. 103, p. 1523-1529.

Pidgeon, R.T., Nemchin, A.A., and Hitchen, G.J., 1998, Internal structures of zircons from Archean granites from the Darling Range batholith: implications for zircon stability and the interpretation of zircon U-Pb ages: Contributions to Mineralogy and Petrology, v. 132, p. 288-299

Reeder, J.V., 2017, Formation of kyanite-bearing migmatites in the central Adirondacks [M.S. thesis]: San Francisco, California, San Francisco State University, 96 p.

Regan, S.P., Walsh, G.J., Williams, M.L., Chiarenzelli, J.R., Toft, M., and McAleer, R., 2019, Syn- collisional exhumation of hot middle crust in the Adirondack Mountains (New York, USA): Implications for extensional orogenesis in the southern Grenville province: Geosphere, v. 15, p. 1240-1261, doi: https://doi.org/10.1130/GES02029.1

Rivers, T., 2008, Assembly and preservation of lower, mid, and upper orogenic crust in the Grenville Province - Implications for the evolution of large hot long-duration orogens: Precambrian Research, v. 167, p. 237-259.

Rivers, T., 2009, The Grenville Province as a large hot long-duration collisional orogen – insights from the spatial and thermal evolution of its orogenic fronts: Geological Society, London, Special Publications, v. 327, p. 405–444.

Rivers, T., 2012, Upper-crustal orogenic lid and mid-crustal core complexes; signature of a collapsed orogenic plateau in the hinterland of the Grenville Province: Canadian Journal of Earth Sciences, v. 49 p.1-42.

Rivers, T., 2015, Tectonic Setting and Evolution of the Grenville Orogen: An Assessment of Progress Over the Last 40 Years: Geoscience Canada, v. 42, p. 77-124.

Rubatto, D., 2002, Zircon trace element geochemistry: partitioning with garnet and the link between U–Pb ages and metamorphism: Chemical Geology, v. 184, p. 123-138, https://doi.org/10.1016/S0009-2541(01)00355-2.

Rubatto, D., Muntener, O., Barnhoorn, A., and Gregory, C., 2008, Dissolution-reprecipitation of zircon at low-temperature, high-pressure conditions (Lanzo Massif, Italy): American Mineralogist, v. 93, p. 1519-1529, https://doi.org/10.2138/am.2008.2874

Rubatto, D., Chakraborty, S., and Dasgupta, S., 2012, Timescales of crustal melting in the Higher Himalayan Crystallines (Sikkim, Eastern Himalaya) inferred from trace element-constrained monazite and zircon chronology: Contributions to Mineralogy and Petrology, https://doi.org/10.1007/s00410-012-0812-y

Rubatto, D., 2017, Zircon: The metamorphic mineral: Reviews in Mineralogy and Geochemsity, v. 83, p. 261-295, https://doi.org/10.2138/rmg.2017.83.9.

Sawyer, E.W., 2008, Atlas of Migmatites: Mineralogical Association of Canada

Siebel, W., Shang, C.K., Thern, E., Danisik, M., and Rohrmuller, J., 2012, Zircon response to high-grade metamorphism as revealed by U-Pb and cathodoluminescence studies: International Journal of Earth Sciences, v. 101, p. 2105-2123, DOI 10.1007/s00531-012-0772-5

Stacey, J.S., and Kramers, J.D., 1975, Approximation of terrestrial lead isotope evolution by a two-stage model: Earth and Planetary Science Letters, v. 26, p. 207–221, https://doi.org/10.1016/0012-821X(75)90088-6.

Shinevar, W.J., Jagoutz, O., and VanTongeren, J.A., 2021, Gore Mountain Garnet Amphibolite Records UHT Conditions: Implications for the Rheology of the Lower Continental Crust during Orogenesis: Journal of Petrology, v. 62, p. egab007, https://doi.org/10.1093/petrology/egab007.

Storm, L.C., and Spear, F.S., 2005, Pressure, temperature and cooling rates of granulite facies migmatitic pelites from the southern Adirondack Highlands, New York: Journal of Metamorphic Geology, v. 23, p. 107-130.

Streepey, M.M., Johnson, E.L., Mezger, K., and van der Pluijm, B.A., 2001, Early History of the Carthage-Colton Shear Zone, Grenville Province, Northwest Adirondacks, New York (U.S.A.): The Journal of Geology, v. 109(4) p. 479-492

Selleck, B.W., McLelland, J.M., and Bickford, M.E., 2005 Granite emplacement during tectonic exhumation: The Adirondack example: Geology, v. 33, p. 781-784

Spear, F.S., and Florence, F.P., 1992 Thermobarometry in granulites: Pitfalls and new approaches: Precambrian Research, v. 55, p. 209-241. https://doi.org/10.1016/0301-9268(92)90025-J

Spear, F.S., and Markussen, J.C., 1997, Mineral zoning, P-T-X-M phase relations, and metamorphic evolution of some Adirondack granulites, New York: Journal of Petrology, v. 38, p.757-783, https://doi.org/10.1093/petroj/38.6.757.

Teyssier, C., and Whitney, D.L., 2002, Gneiss domes and orogeny: *Geology*, v. 30 (12), p. 1139-1142. doi: https://doi.org/10.1130/0091-7613(2002)030<1139:GDAO>2.0.CO;2

Valentino, D.W., Chiarenzelli, J.R., and Regan, S.P., 2018, Spatial and temporal links between Shawinigan accretionary orogenesis and massif anorthosite intrusion, southern Grenville Province, New York, U.S.A.: Journal of Geodynamics, v. 129, p. 80-97

Vermeesch, P., 2018, IsoplotR: A free and open toolbox for geochronology: Geoscience Frontiers, v. 9, p. 1479-1493, https://doi.org/10.1016/j.gsf.2018.04.001.

Werner, C.D., 1987, Saxonian granulites — A contribution to the geochemical diagnosis of the original rocks in high-metamorphic complexes: Gerlands Beiträge zur Geophysik, v. 96, p. 271-290.

Whalen, J.B., Currie, K.L., and Chappell, B.W., 1987, A-type granites: Geochemical characteristics, discrimination and petrogenesis: Contributions to Mineralogy and Petrology, v. 95, p. 407-419, https://doi.org/10.1007/BF00402202.

Whitney, D.L., and Evans, B.W., 2010, Abbreviations for names of rock-forming minerals: The American Mineralogist, v. 95, p. 185-187, https://doi.orrg/10.2138/am.2010.3371.

Williams, I.S., 1998, U-Th-Pb geochronology by ion microprobe, *in* McKibben, M.A., Shanks, W.C., III, and Ridley, W.I., eds., Applications of Microanalytical Techniques to Understanding Mineralizing Processes: Society of Economic Geology, Reviews in Economic Geology, v. 7, p. 1-35, https://doi.org/10.5382/Rev.07.01.

Wong, M.S., Williams, M.L., McLelland, J.M., Jercinovik, M.J., and Kowalkoski, J., 2012, Late Ottawan extension in the eastern Adirondack Highlands: Evidence from structural studies and zircon and monazite geochronology: Geological Society of America Bulletin, v. 124, p. 857-869, https://doi.org/10.1130/B30481.1.

ABBREVIATIONS

AMCG - Anorthosite mangerite charnockite granite
BSE - backscattered electron
CCSZ - Carthage Colton shear zone
CL - cathodoluminescence
EASZ - East Adirondack shear zone
EDMAP - educational map
HL - highlands
HREE - Heavy rare-earth elements
ICP-MS - inductively coupled plasma mass spectrometry
LL - lowlands
LM - Ledge Mountain
LREE - Light rare-earth elements
MREE - Middle rare-earth elements
OZP - Oscillatory zoning pattern
PLSZ - Piseco Lake shear zone
P-T - pressure- temperature
REE - Rare Earth Elements
SEM - scanning electron
SHRIMP - Sensitive high resolution Ion Microprobe
UHT - Ultra-high temperature
USGS - U.S. Geological Survey
XRF - x-ray fluorescence

APPENDICES

Appendix I. Geologic timeline with Zircon U-Pb ages

Geologic eras are listed to understand timing of geologic events in the Adirondacks. Zircon ages for all of the sampled rocks are listed.

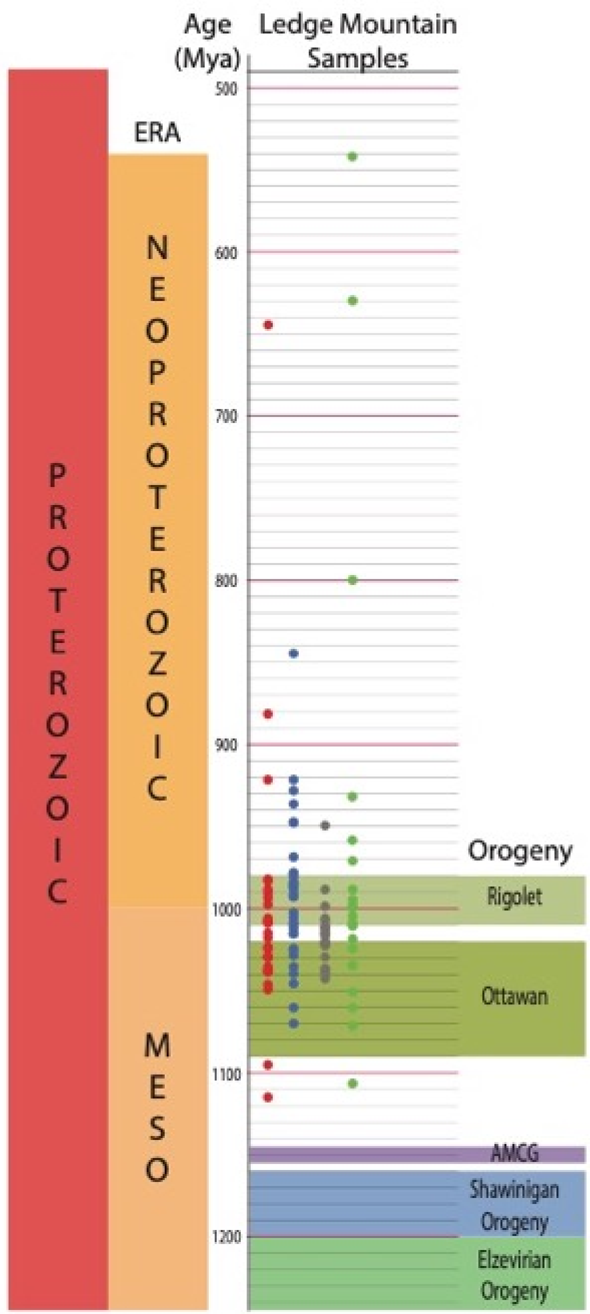

Appendix II. Supplemental text for the section "SAMPLE SELECTION, ANALYTICAL METHODS & RESULTS"

Field Work

I completed 3 weeks of field research in August 2021. I mapped the central part of the Rock Lake quadrangle north of Indian Lake, NY, and collected samples for petrography and U-Pb geochronology. The southern face of the Ledge Mountain is steep, nearly vertical at points, so the only access to LM is from the western side of the Rock River trail. Ledge Mountain is ~0.5 miles east of the Rock River trailhead in Indian Lake, NY. Rock exposure is poor and outcrops have a weathered rind that makes sampling difficult. Rock is only exposed near the top elevations, along the steep cliff face and in a few prominent cliffs that strike nearly east-west found along the eastern branch. There are few trails in the Ledge Mountain area, and steep terrain, dense brush/forest, and the presence of marshes, rivers, and lakes make access difficult. The app *StraboSpot* was used to document and georeference field notes, GPS coordinates, and photos. Strikes and dips of foliations were taken using a Brunton geological compass and the app *Rock'd*; these measurements were added in *StraboSpot.* We created 1:12,000 geologic and structural maps of the central Rock Lake quadrangle, and collected 38 samples for petrography and U-Pb geochronology. We collected 20 samples from Ledge Mountain, primarily from the eastern branch of Ledge Mountain.

SHRIMP U-Pb geochronology

SHRIMP is ideally used to study these structurally and chemically complex zircons because it allows minimally destructive repeated sampling of domains for isoptic and trace element analyses (Wooden et al., 2006; Barth and Wooden, 2010). There are many situations where it is desirable to focus on the outermost 2-5 microns of mineral growth. These types of analyses are most commonly performed on relatively young zircons (<300 ka) where the youngest age of zircon growth is targeted. However, in practice, depth profiling can be done on almost any material for U-Th or U-Pb or Th-Pb ages and/or trace element analyses. Mount preparation requires pressing flat, unpolished, mineral surfaces into soft indium metal. If the grains have adhering glass or other particles, the samples may need to be rinsed in dilute HF to clean the sample surfaces. Three to six rows of sample and standard grains (40-80 individual grains) are carefully arranged on a glass slide covered in a thin layer of vacuum grease. The grease allows grains to be easily rotated to align flat grain surfaces. The grains are pressed into polished indium metal, which has been pushed into 4 mm x 12 mm troughs milled into 25.4 mm diameter polished epoxy or aluminum disk. The samples have to be carefully cleaned with soap and 1M HCl with great care not to pluck out grains, thoroughly rinsed in de-ionized water, and dried in a vacuum oven for approximately half hour. Unpolished indium mounted grains can also be carefully polished to expose the grain interiors and re-analyzed for depth-profiling sections or to obtain ages of mineral "cores."

Before SHRIMP analysis, CL and BSE images were used to identify different compositional zones within individual grains to be tested and areas with inclusions and cracks to be avoided. SEM images were used to identify physical defects in the "topography" of the mounts to avoid and flat areas to target. Grains were re-imaged after analysis to evaluate for errors with the beam spot location. The mounted grains were washed with a 1N HCl solution and thoroughly rinsed in distilled water, dried in a vacuum oven, and coated with gold prior to analysis. The mounts were stored at high vacuum (10^{-7} torr) for several hours before being moved into the source chamber of the SHRIMP-RG to minimize degassing of the epoxy and isobaric hydride interferences and masses 204-208.

Secondary ions were sputtered from the target spot using an O_2^- primary ion beam, which had an intensity varying from 2.0 to 2.3 nA. The primary ion beam spot had an ellipse-shape approximately 22 x 24 microns and a depth of ~1.0 micron for the analyses performed in this study. Before every analysis, the sample surface was cleaned by rastering the primary beam for 60 seconds, and the primary and secondary beams were auto-tuned to maximize transmission. The acquisition routine includes analysis of $^{30}Si^{16}O^+$, $^{48}Ti^+$, $^{49}Ti^+$, $^{56}Fe^+$, $^{89}Y^+$, 9-REE ($^{139}La^+$, $^{140}Ce^+$, $^{146}Nd^+$, $^{147}Sm^+$, $^{153}Eu^+$, $^{155}Gd^+$, $^{162}Dy^{16}O^+$, $^{166}Er^{16}O^+$, $^{172}Yb^{16}O^+$), a high mass normalizing species ($^{90}Zr_2{}^{16}O^+$), followed by $^{180}Hf^{16}O^+$, $^{204}Pb^+$, a background measured at 0.045 mass units above the $^{204}Pb^+$ peak, $^{206}Pb^+$, $^{207}Pb^+$, $^{208}Pb^+$, $^{232}Th^+$, $^{238}U^+$, $^{232}Th^{16}O^+$, and $^{238}U^{16}O^+$, $^{238}U^{16}O_2{}^+$. Trace element measurements (Ti, Fe, Y, Hf, REE) are measured briefly (typically 1 to 5 sec/mass) immediately before the geochronology peaks, and in mass order. For the first session, $^{232}Th^+$ was not measured. All peaks are measured on a single EPT® discrete-dynode electron multiplier operated in pulse counting mode with 5 scans (peak-hopping cycles from mass 46 through 270). The counting times on each peak are varied according to the sample age and the U and Th concentrations to improve counting statistics and age precision. Measurements are made at mass resolutions of $M/\Delta M$ = 8600-9000 (10% peak height), which eliminates interfering molecular species, particularly for the REE.

Zircon concentration data for U, Th and all measured trace elements are calculated relative to MAD (4196 ppm U; Barth and Wooden, 2010). Calculated model ages for zircon are standardized relative to R33 (419 Ma; Black et al., 2004), which was analyzed repeatedly throughout the duration of the analytical session. The original data reduction for geochronology follows the methods described by Williams (1998), and Ireland and Williams (2003), and uses the MS Excel add-in programs Squid2.51 and Isoplot3.764 of Ludwig (2009, 2012). Calculations of weighted mean ages included in this paper used IsoplotR (Vermeesch, 2018).
The measured $^{206}Pb/^{238}U$ was corrected for common Pb using ^{207}Pb, whereas $^{207}Pb/^{206}Pb$ was corrected using ^{204}Pb. The common-Pb correction was based on a model Pb composition from Stacey and Kramers (1975). All reported $^{206}Pb/^{238}U$ and $^{207}Pb/^{206}Pb$ model ages and uncertainties (2σ) include error summed in quadrature from the external reproducibility of the standard Temora-2 during an individual analytical session (~24 hours).

Data reduction for the trace element concentrations are performed in MS Excel. Average count rates of each element of interest are ratioed to $^{30}Si^{16}O$ to account for any primary current drift, and the derived ratios for the unknowns are compared to an average of those for the standards to determine concentrations. Spot to spot precisions (as measured on the standards) vary according to elemental ionization efficiency and concentration. For the MADDER zircon, precisions generally range from about ± 3% for Hf, ± 5-10% for the Ti, Fe, Y and HREE, ± 10-15%, and up to ± 40% for La which is present most often at the ppb level (all values at 2σ) (Coble et al., 2018).

Fe is naturally low in zircon (<~10 ppm). Trace element analyses with high concentrations of Fe (>~1000 ppm) as well as high concentrations of Ti likely result from errors in measurement and were omitted from data analysis. In addition, high common Pb and topographical variation on zircon grains due to cracks or beam spots overlapping with inclusions were criteria used to omit unreliable analyses (age, compositional, temperature analyses from the same beam location) as these analyses do not accurately reflect the zircon composition.

I measured a set of trace elements and Ti-in-zircons with the SHRIMP-RG. Measured trace element compositions were chondrite-normalized using McDonough and Sun (1995). Normalized concentrations were plotted against atomic number on a spider diagram, to see compositional trends (enrichment/depletion, the steepness of positive or negative slopes or plateaus) or anomalous elemental concentrations (Fig. 7-8).

Appendix III. Cathodoluminescence images of all zircons

Four images displaying all of the analyzed zircons are included for reference.


AD01-1.1
997.40±12.71
AD01-2.1
660.33±11.69
AD01-3.1
1035.51±12.76
AD01-4.1
1035.29±12.54
AD01-5.1
1051.67±8.78
AD01-6.1
1027.77±6.24
AD01-7.1
1054.38±11.44
AD01-8.1
1044.77±7.17
AD01-9.1
1035.18±23.16
AD01-10.1
1043.07±19.52
AD01-11.1
1000.73±9.45
AD01-12.1
990.34±5.35
AD01-13.1
1004.19±14.63
AD01-14.1
995.07±12.40
AD01-15.1
1014.45±11.65
AD01-16.1
930.18±7.52
AD01-17.1
989.55±17.81
AD01-18.1
1014.57±19.57
AD01-19.1
1041.04±6.56
AD01-20.1
1099.55±16.68
AD01-21.1
1016.25±11.58
AD01-22.1
1042.72±12.42
200 microns
AD01
AD01-23.1
1012.77±16.27
AD01-24.1
891.36±15.00
AD01-25.1
1030.21±17.96
AD01-26.1
1035.39±11.13
AD01-27.1
1118.21±21.13
AD01-28.1
1027.77±6.24
AD01-29.1
1032.91±26.48

17LM01-1.1
1013.62 ±15.63
17LM01-1.2
992.67±14.19
17LM01-2.1
1017.7±5.9
17LM01-3.1
995.81±14.1
17LM01-4.1
998.49±18.5
17LM01-5.1
1045.8±48.22
17LM01-6.1
1031.33±11.39
17LM01-7.1
1051.98±13.25
17LM01-8.1
994.83±21.79
17LM01-8.2
930.18±34.15
17LM01-9.1
944.41±16.55
17LM01-10.1
1034.24±12.51
17LM01-11.1
987.61±6.41
17LM01-12.1
1021.01±10.21
17LM01-13.1
956.35±17.36
17LM01-14.1
993.33±13.42
17LM01-15.1
855.92±40.67
17LM01-16.1
988.87±10.8
17LM01-17.1
1041.04±5.64
17LM01-18.1
985.89±17.27
17LM01-19.1
955.01±45.4
17LM01-20.1
937.92±12.55
17LM01-21.1
1008.19±12.88
17LM01-22.1
999.88±15.04
17LM01-23.1
991.37±8.93
17LM01-24.1
976.97±27.7
17LM01-25.1
1030.29±11.35
17LM01-26.1
1065.51±15.61
17LM01-27.1
1015.55±16.9
17LM01-28.1
1021.7±12
17LM01-29.1
1018.8±46.37
17LM01-30.1
1074.09±6.89
17LM01
200 microns


17LM07
200 microns
17LM07-1.1
1046.74±12.50
17LM07-2.1
1017.91±15.54
17LM07-3.1
1043.47±16.33
17LM07-4.1
1013.71±11.88
17LM07-5.1
1042.81±9.11
17LM07-6.1
1021.96±10.24
17LM07-7.1
1011.43±14.62
17LM07-8.1
1019.10±13.35
17LM07-9.1
958.63±5.78
17LM07-10.1
1028.29±11.17
17LM07-11.1
1027.77±6.24
17LM07-12.1
1028.98±13.23
17LM07-13.1
1026.13±9.8
17LM07-14.1
1018.75±18.62
17LM07-15.1
1005.45±13.75
17LM07-16.1
1021.45±16.73
17LM07-17.1
994.69±6.16
17LM07-18.1
1036.75±8.15
17LM07-19.1
1049.72±14.47
17LM07-20.1
1023.11±6.32


17LM14
17LM14-15.1
1015.95±11.17
17LM14-4.1
1006.8±14.94
17LM14-1.1
1012.73±10.48
17LM14-2.1
995.83±7.02
17LM14-3.1
1017.97±5.53
17LM14-16.1b
966.15±23.41
17LM14-5.1
1004.75±12.54
17LM14-6.1
560.38±10.3
17LM14-7.1
1040.28±17.45
17LM14-8.1
942.34±6.27
17LM14-9.1
812.43±40.55
17LM14-10.1
646.89±10.56
17LM14-11.1
1018.98±12.89
17LM14-12.1
1076.27±6.29
17LM14-13.1
1024.3±14.84
17LM14-14.1
1030±10.48
200 microns
17LM14-16.1a
978.94±8.14
17LM14-17.1
1056.25±12.15
17LM14-18.1
1056.25+12.15
17LM14-19.1
1067.48±16.05
17LM14-20.1
1001.46±28.28
17LM14-21.1
1110.34±8.86